UNIVERSITY OF BENIN

P.M.B. 1154, BENIN CITY, EDO STATE

DESIGN AND ANALYSIS OF HEAT EXCHANGERS USING TRIPLY PERIODIC MINIMAL SURFACES (TPMS)

BY;

SAMUEL TAM DEINDUOMO	**ENG2009607**
OGHENEMARO MAJIRIOGHENE OKPIGHE	**ENG2002497**
ABRAHAM EWERE FRED	**ENG2006380**

SUBMITTED TO;

THE DEPARTMENT OF MECHANICAL ENGINEERING

IN PARTIAL FULFILMENT OF THE REQUIREMENT FOR BACHELOR OF ENGINEERING (B. ENG) IN MECHANICAL ENGINEERING

FACULTY OF ENGINEERING

NOVEMBER 2025

SUPERVISOR:

PROF. S. A. ALIU

CERTIFICATION

This is to certify that this research project titled: **DESIGN AND ANALYSIS OF HEAT EXCHANGERS USING TRIPLY PERIODIC MINIMAL SURFACES (TPMS)** submitted to the Department of Mechanical Engineering was carried out by **Samuel Tam Deinduomo**, **Oghenemaro Majirioghene Okpighe** and **Abraham Ewere Fred** of the Department of Mechanical Engineering, University of Benin, Benin city, Edo State, Nigeria, under the supervision of **Prof. S. A. Aliu.**

…….. ……

Prof. S. A. Aliu **Date**

Project Supervisor

…….. ……

Engr. Martin Oshikueme **Date**

Project Coordinator 2024/2025

…….. ……

Prof. O. O. Ighodaro **Date**

Head of Department

DEDICATION

We dedicate this project to God and to our loved ones: our family and friends. Your unwavering support has been invaluable, and we are profoundly grateful for the privilege of your encouragement.

ACKNOWLEDGMENT

We wish to express our profound gratitude, first and foremost, to God Almighty for granting us the strength, wisdom, and opportunity needed to carry out this project. We would also like to extend our heartfelt thanks to our respective families for their constant love, support, and patience throughout this journey.

Our sincere gratitude goes to our supervisor, Prof. S. A. Aliu, who deemed us fit to undertake such a novel topic. Your unwavering support, insightful guidance, and words of encouragement have made this project both an enriching learning experience and a truly rewarding endeavour.

We are deeply appreciative of the individuals and organizations who generously provided journals, resources, data, and valuable insights that significantly enhanced our research and analysis.

Lastly, we extend our sincere thanks to everyone who contributed to this project, whether directly or indirectly. In particular, we would like to acknowledge Engr. Martin Oshikueme, our project coordinator, for his guidance and consideration throughout this entire process.

ABSTRACT

Conventional heat exchangers face a fundamental trade-off between thermal effectiveness and hydraulic performance. Triply Periodic Minimal Surfaces (TPMS), enabled by Additive Manufacturing, present a promising solution, offering high surface-to-volume ratios and complex internal geometries that promote enhanced flow mixing and heat transfer. This research details the design and numerical analysis of a heat exchanger utilizing a Gyroid TPMS core. The primary objective was to assess its thermal-hydraulic performance using Computational Fluid Dynamics (CFD) and benchmark it against a conventional plate-type exchanger.

The methodology employed a novel computational workflow, beginning with the generation of the complex implicit geometry in nTopology. This model was then exported to Ansys Fluent for simulation. A full-scale Conjugate Heat Transfer (CHT) analysis was conducted, using the k-ω SST turbulence model to accurately resolve the flow and thermal coupling. The intricate geometry's meshing challenge was overcome using the Fault-Tolerant Meshing (FTM) workflow.

The validated simulation results demonstrated the superior hydrodynamic efficiency of the Gyroid TPMS design with a 1370% lower pressure drop and 570% less pumping power. This presented a clear trade-off, as the conventional plate-type transferred 2.4 times more heat but at a substantial pressure cost. This study successfully validates a robust computational workflow for analysing complex TPMS geometries and concludes that these architectures provide a viable path toward developing more compact, lightweight, and thermally efficient heat exchangers.

TABLE OF CONTENTS

LIST OF FIGURES

LIST OF TABLES

NOMENCLATURE / ABBREVIATIONS

Symbol	Description	Units
Latin Symbols		
A	Area / Surface area	mm²
A_{sf}	Total solid - fluid interaction area	mm²
a_{sf}	Specific solid - fluid interaction area	1/mm
C	Heat capacity rate	W/K
Cr	Heat capacity rate ratio	—
C_p	Specific heat capacity	J/(kg·K)
D	Diameter	m
Dh	Hydraulic diameter	m
f	Friction factor	—
g	Acceleration due to gravity	m/s²
h	Heat transfer coefficient OR Specific enthalpy	W/(m²·K) OR J/kg
V	Overall heat transfer coefficient	W/(m²·K)
L	Length	m
$\dot{m}$	Mass flow rate	kg/s
$\dot{P}$	Pumping power	W
p	Pressure	Pa
$\dot{Q}$	Heat transfer rate	W
q''	Heat flux	W
Rcond	Thermal resistance of solid wall due to conduction	K/W or °C/W
Rc,conv	Thermal resistance of cold fluid due to convection	K/W or °C/W
Rh,conv	Thermal resistance of hot fluid due to convection	K/W or °C/W
s	Specific entropy	J/(kg·K)
T	Temperature	K
T_0	Reference temperature	K
V	Volume	m³

$\dot{V}$	Volumetric flow rate	m³/s or dm³/min
Vs	Enclosed (wetted) volume	m³
v	Velocity	m/s
Greek Symbols		
Δp	Pressure drop	Pa
ΔT	Temperature difference	K
ΔT_{LMTD}	Log Mean Temperature Difference	K or °C
ε	Effectiveness / Temperature effectiveness	—
η_p	Pump efficiency	—
k_f	fluid thermal conductivity	W/mK
λ_{eff}	Effective thermal conductivity	W/mK
μ	Dynamic viscosity	kg/(m·s) or Pa·s
ν	Kinematic viscosity	m²/s
ρ	Density / Fluid density	kg/m³
ϕ	Porosity	—
Dimensionless Numbers		
Nu	Nusselts number	—
NTU	Number of transfer units	—
Pr	Prandtl number	—
Re	Reynolds number	—
Subscripts		
c	Refers to cold fluid	—
h	Refers to hot fluid	—
in	Refers to inlet	—
max	Maximum	—
min	Minimum	—
out	Refers to outlet	—

CHAPTER 1

INTRODUCTION

The focus of this research is to design a Heat Exchanger, utilizing a Triply Periodic Minimal Surface (TPMS) structure as the core internal geometry. The research aims to assess and characterize the thermal-hydraulic performance of the TPMS-based heat exchanger numerically through Computational Fluid Dynamics (CFD) simulations. The study will evaluate key performance metrics such as heat transfer efficiency and pressure drop to assess the feasibility of TPMS geometries in enhancing heat exchanger effectiveness. This investigation seeks to establish whether TPMS structures offer a superior trade-off between thermal effectiveness and hydraulic performance compared to conventional exchanger configurations.

1.1. BACKGROUND TO THE STUDY

The demand for efficient, compact, and structurally robust heat exchangers has intensified across several engineering applications, including aerospace propulsion systems, supercritical CO_2 power cycles, microelectronic thermal management amongst many others (Li et al., 2022; Sun et al., 2021). Traditional heat exchangers are designed using subtractive manufacturing techniques where bulk materials are machined, joined or formed into internal structures such as fins, tubes, or corrugated plates. While these conventional designs have been deployed across industries, they exhibit fundamental limitations, chiefly; geometric complexity, part assembly constraints, and thermal durability at extreme operating conditions (Bayomy et al., 2022). Modular construction often introduces mechanical joints which introduce discontinuities in surface contact, thereby compromising structural integrity and thermal continuity, particularly in high-pressure or high-temperature environments (King et al., 2015; Khrapov et al., 2021).

As identified in recent literature, a significant limitation of these conventional designs is their inability to simultaneously optimize thermal performance and pressure drop. Attempts to enhance heat transfer often involve increasing the internal surface area by adding fins, corrugations and internal inserts which, while beneficial for convection,

leads to a rise in flow resistance and mechanical complexity while flowing through narrower or more tortuous passages (Bhattacharya et al., 2021; Attarzadeh et al., 2020). Higher pressure drops translate into greater pumping power requirements, reducing the overall system efficiency. Thus, efforts to improve thermal efficiency often come at the expense of hydraulic performance, forcing designers into a constant trade-off between competing objectives. Moreover, manufacturing constraints restrict the internal geometries that can be realized using traditional fabrication methods, preventing the full exploitation of spatial design for improved flow mixing and heat transfer (Kumar et al., 2022; Tandel, 2022). As a result, the design space for conventional Heat Exchangers is artificially restricted to geometries that are feasible to manufacture, rather than geometries that might offer the best heat transfer performance. Additionally, to physically improve the effectiveness and performance of conventional Heat Exchangers, the heat transfer surface geometry is made larger, undermining the compactness requirements of modern thermal systems. The need for tight tolerances and careful alignment of parts in standard designs increases both manufacturing costs and assembly time.

These limitations underscore the need for a new class of heat exchanger geometries that can balance thermal efficiency with hydraulic performance and structural integrity. The emergence of Additive Manufacturing (AM) has opened a pathway for such designs, particularly through the integration of Porous Media as internal structures, which offer interconnected, smoothly curved internal channels with high surface-to-volume ratios and favourable flow development characteristics (Al Ketan et al., 2021), yet their fabrication and thermal evaluation remain underexplored in mainstream industrial practice.

Additive Manufacturing offers advantages of allowing for rapid and inexpensive prototyping, the design and manufacture of Heat Exchangers with lower surface area to volume ratios. AM HXs are lighter, compact and manufactured as one piece, which reduces likelihood of failure due to potential points of weakness such as mechanical joints, load paths, and assembly tolerances. However, replacement of faulty parts is not an option. Additive Manufacturing has the potential to significantly alter the thermal-hydraulic design trade-off, as the process can realize intricate, smoothly curved internal geometry that promote mixing, optimize flow distribution, and maximize surface-to-volume ratios without introducing excessive pressure drop. A particular promising class

of Porous Media in this regard are the Triply Periodic Minimal Surfaces, as heat transfer surfaces, which offer the benefits and drawbacks of Heat Exchangers designed with additive manufacturing methods. Triply Periodic Minimal Surfaces (TPMS) can be described as porous cellular-like structures that can categorically be governed by mathematical equations made up of trigonometric functions. They possess unique characteristics which offer a large surface area - to - volume ratio and a zero-mean curvature at every point on the surface. They are characterized by their smooth edge-and-corner-free geometries and their ability to divide space into non-intersecting and intertwined, infinite, periodic domains in three perpendicular directions.

Despite these advantages, TPMS HXs remain relatively underexplored in commercial engineering practice. While laboratory-scale demonstrations have shown promising thermal and structural characteristics, challenges remain in scaling up fabrication, ensuring repeatable material properties, and integrating such designs into established commercial standards. Nevertheless, the opportunities outweigh the challenges. Additive manufacturing enables lightweight, compact, and geometrically optimized heat exchangers that address many of the shortcomings of conventional designs. When combined with TPMS architectures, AM provides a pathway to next-generation Heat Exchangers capable of delivering superior thermal efficiency, manageable hydraulic performance, and robust structural integrity, all within a compact and manufacturable package. As industrial adoption of AM expands, and computational tools for optimizing TPMS geometries mature, it is likely that these designs will transition from research prototypes to mainstream engineering solutions.

1.2. PROBLEM STATEMENT

Prior work on TPMS heat exchangers, largely excluded working fluids such as oils and liquid metals, despite their relevance in advanced energy and industrial applications. Another critical limitation is the absence of unified performance benchmarking across TPMS geometries. With no standardized test conditions or comparative datasets, the selection of optimal topology for specific applications remains ad hoc. Thermofluidic investigations further reveal that geometry-flow regime interactions govern heat transfer outcomes more strongly than global porosity or surface area, complicating predictive design. Most importantly design often proceeds without commercial process considerations, limiting practical adoption of TPMS heat exchangers.

1.3. AIMS & OBJECTIVES

1.3.1. AIMS

This study aims to develop and evaluate heat exchangers using TPMS geometries optimized for commercial applications.

1.3.2. OBJECTIVES

The specific objectives include;

1. To conduct a literature review of TPMS Heat Exchanger design and analysis utilizing both experimental and computational studies.
2. The generation of TPMS-based heat exchanger model.
3. Simulation of conjugate heat transfer and flow behaviour within these TPMS cores.
4. Systematic variation of boundary conditions to assess their influence on thermal gradients and pressure loss.
5. Model validation by comparing results against experimental and numerical data from literature.

1.4. SCOPE OF THE STUDY

The study focuses exclusively on the design and numerical investigation of TPMS heat exchangers. The scope is confined to single-phase, steady-state flow simulations using computational fluid dynamics with Reynolds numbers which represent flow regimes typical of commercial processes. Computational models assume ideal material properties, uniform thermal conductivity and neglect fouling, and material degradation effects. The study excludes conventional heat exchanger geometries from direct simulation but uses established performance metrics from the literature as comparative baselines, hence, no experimental fabrication of the HX is undertaken. These simplifications enable a focused examination of core geometry on thermal and hydraulic behaviour within the TPMS cores.

1.5. SIGNIFICANCE OF THE STUDY

This research addresses critical challenges in the design of next-generation heat exchangers by evaluating the thermofluidic performance of TPMS structures. As highlighted in the literature, conventional heat exchangers are constrained by geometry, manufacturability, and pressure drop penalties that limit their effectiveness under extreme operating conditions. TPMS geometries, enabled by additive manufacturing,

present an opportunity to overcome these barriers through their high connectivity, smooth internal surfaces, and geometric adaptability.

The significance of this work lies in its contribution to a growing field of thermal systems research that seeks to integrate computational modelling, geometric optimization, and additive manufacturing. By establishing a rigorous comparative framework between TPMS and conventional core geometries, this study provides valuable insights into their potential for thermal management in high-performance systems. The findings serve to inform future research in heat exchanger design, supporting innovation in commercial sectors such as power generation, electronics cooling, aerospace propulsion and so on.

1.6. LIMITATIONS OF THE STUDY

The primary limitation of the study is its exclusive reliance on computational modelling. The CFD simulations assume ideal boundary conditions and neglect physical phenomena such as fouling deposition, and structural anisotropy induced during additive manufacturing. These phenomena, while present in real-world systems, are outside the scope of this study due to constraints in physical prototyping and validation facilities. The turbulence models employed in the simulation, while standard in engineering practice, introduce approximations that may not fully capture the local eddy dynamics and heat flux variations observed in experimental settings. These limitations suggest that while the study provides a robust theoretical foundation, additional experimental and post-processing investigations are needed to validate the performance and durability of TPMS heat exchangers under operational loads.

CHAPTER 2

LITERATURE REVIEW

This chapter establishes the conceptual, theoretical and technical foundation for the TPMS Heat Exchanger design and analysis by describing in detail, the history, advances and applicable fabrication techniques.

2.1. CHARACTERIZATION

Characterization in porous heat exchanger design involves the systematic evaluation of attributes governing thermo-hydraulic performance:

1. Geometric characterization involves describing porosity, surface area-to-volume ratio, curvature, and pore size distribution, which determine flow pathways and heat transfer interfaces (Maconachie et al., 2019).
2. Hydraulic characterization focuses on parameters such as permeability, pressure drop, and friction factor, since tortuosity and surface roughness directly influence pumping power and flow uniformity (Kaviany, 1995).
3. Thermal characterization evaluates effective thermal conductivity, Nusselt number correlations, and temperature distribution across the porous matrix, reflecting the balance between heat transfer enhancement and energy penalties (Lu et al., 2000).

   These dimensions enable performance benchmarking and guide optimization strategies in design-for-additive-manufacturing.

2.2. HEAT EXCHANGERS

The process of heat exchange between two fluids that are at different temperatures and separated by a solid wall occurs in many engineering applications. The device used to implement this exchange is termed a Heat Exchanger (HX), and specific applications may be found in space heating and air-conditioning, power production, waste heat recovery, and chemical processing.

Heat exchangers are commonly classified by flow arrangement and construction type. The simplest is the concentric tube exchanger, operating in parallel, counterflow, or crossflow modes, with counterflow providing the greatest temperature difference. Construction types include tubular, extended surface, plate-and-frame, and regenerative designs. The shell-and-tube exchanger is widely used, employing baffles to enhance heat transfer and limit vibration. Compact exchangers provide very high surface-area-

to-volume ratios, using finned or corrugated structures to improve performance when one fluid has low convection coefficients (Incropera & DeWitt, 2007).

2.3. POROUS MEDIA

Porous media are materials characterized by a solid matrix interspersed with interconnected voids or pores that allow the passage of fluids. These structures can be natural, such as bone or coral, or synthetic, including foams, lattices, and additively manufactured periodic surfaces. Their defining feature is the combination of high surface area, tortuous flow pathways, and tunable porosity, which enable enhanced heat and mass transfer compared to bulk materials. Porous media can be categorized into two main types: periodic (regular) and stochastic (irregular) structures, distinguished primarily by the arrangement of pores (Xu et al., 2015).

Cellular structures commonly exist as foams or lattices. Foam architectures are preferred for high energy absorption, stiffness, and strength, while lattice structures offer greater control over deformation (Sharma & Hiremath, 2021). In heat exchangers, porous cores enhance effective thermal conductivity and heat capacity, improving power density and overall system efficiency (Delalic et al., 2004). Additive manufacturing enables highly complex porous geometries in metals such as aluminium and copper. Aluminium foams, for example, have demonstrated heat transfer rates up to forty times higher than hollow tubes under turbulent flow (Lu et al., 2000). However, these performance gains must be balanced against increased pressure drop and associated pumping power requirements.

2.4. TRIPLY PERIODIC MINIMAL SURFACES (TPMS)

A peculiar type of periodic porous structure, Triply Periodic Minimal Surfaces (TPMS) have gained prominence in heat exchanger design (Feng et al., 2022). They are mathematical constructs represented by implicit functions that yield intricately curved surfaces capable of dividing a given domain into two distinct labyrinth-like structures. Minimal surfaces defined in the language of differential geometry are surfaces of zero mean curvature. This means they are equally convex and concave at all points and their form is therefore saddle–like or hyperbolic.

They are called minimal because given a fixed boundary curve, the area of a minimal surface is extremal with respect to other surfaces with the same boundary. The defining

characteristic of a minimal surface is its zero-mean curvature, meaning that the sum of principal curvatures equals zero (Gao et al., n.d.). Consequently, minimal surfaces possess the unique property of minimizing the local area they cover within the domain.

While being mathematically defined surfaces TPMS are encountered in nature (Al-Ketan & Abu Al-Rub, 2019), the simplest of the minimal surfaces is the catenoid, discovered by Euler in 1744, and can be realized by a soap film between two parallel wire rings, with the film stretched between them, narrow at the centre, and flaring out to match the ring edges.

2.5. HISTORY OF TRIPLY PERIODIC MINIMAL SURFACES

The first TPMS surfaces, Primitive and Diamond surfaces, were described by German Mathematician Scharwz in 1865, followed by a surface described by his student E.R. Neovius in 1883. In 1970, more minimal surfaces, originally referred to as Infinite Periodic Minimal Surfaces (IPMS), such as Gyroid and I-WP surfaces, were described by Alan H. Shoen. In 1987, Fischer and Koch made further contributions with the description of Fisher-Koch S-type surface amongst others. While Schoen's surfaces became popular in natural science the construction was not associated to a mathematical existence proof and remained largely unknown in mathematics, until H. Karcher proved their existence in 1989.

Initially introduced in mathematics and later extended to internal flow and heat transfer applications (Jung & Torquato, 2005; Slaughter, 2013), TPMS structures offer large surface-to-volume ratios, zero mean curvature, and self-supporting geometries that simplify manufacturing while providing structural integrity (Peng et al., 2019). Their complex flow patterns intensify mixing, disrupt boundary layers, and enlarge effective heat transfer area (Li et al., 2020). Comparative studies show TPMS geometries such as Diamond, Gyroid, and I-WP significantly outperform conventional finned models, with the Diamond structure often exhibiting the highest convective performance due to enhanced wall-fluid interactions (Tang et al., 2023). Importantly, TPMS can partition 3D domains into distinct but interconnected flow channels, enabling efficient thermal exchange with reduced fouling and hydrodynamic resistance. Practical implementation was historically limited by manufacturing complexity, but additive manufacturing has enabled their production and broadened applications in tissue engineering (Giannitelli

et al., 2014), acoustics (Deshmukh et al., 2019), chemical engineering (Baena-Moreno et al., 2021).

2.6. MATHEMATICAL GENERATION OF TRIPLY PERIODIC MINIMAL SURFACES

Since TPMS are implicit surfaces their geometry can be expressed with equations of the form:

$$f(x, y, z) = C \tag{2.1}$$

Methods used to generate TPMS geometries include

1. **Enneper–Weierstrass parametrical representation**:

$$\begin{cases} x = \Re\left(\int_\gamma (1 - t^2)R(t)dt\right) \\ y = \Re\left(\int_\gamma i(1 + t^2)R(t)dt\right) \\ z = \Re\left(\int_\gamma 2tR(t)dt\right) \end{cases} \tag{2.2}$$

$R(t)$ is the Weierstrass function for different kinds of TPMS units. For the Gyroid, Primitive and Diamond surface its value is:

$$R(t) = \sqrt{\frac{1}{t^8 - 14t^4 + 1}} \tag{2.3}$$

2. **Implicit Function Formulation**:

TPMS can also be generated by the following equation:

$$\phi(r) = \sum_{i=1}^{3} A_i \cos(k_i \cdot r + \varphi_i) - C \tag{2.4}$$

Where A_i is the amplitude, k_i is the period factor and φ_i is the function phase. From these equations we can extrapolate that k influences the TPMS period and C influences the surface. The parameter C determines the porosity of the two

domains generated by the surface. When $C = 0$, the space is divided into two equal, interpenetrating regions, which closely approximate a truly minimal surface. Although these functions do not describe surfaces of constant mean curvature exactly, they provide an excellent approximation for engineering applications and are useful in topology optimization studies.

Different equations can express different types of TPMS:

i. **Gyroid**

$$f(x, y, z) = \sin(\omega x)\cos(\omega y) + \sin(\omega y)\cos(\omega z) + \sin(\omega z)\cos(\omega x) = C \quad (2.5)$$

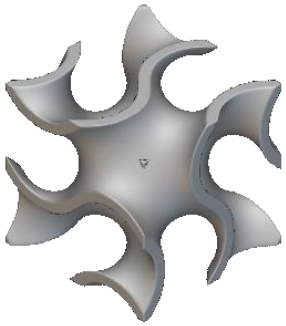

Figure 2.1:*Visual Representation of the Gyroid structure*

ii. **Primitive**

$$f(x, y, z) = \cos(\omega x) + \cos(\omega y) + \cos(\omega z) = C \quad (2.6)$$

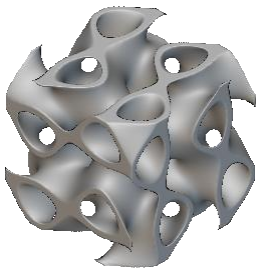

Figure 2.2: *Visual Representation of the Primitive (splitP) structure*

iii. **Diamond**

$$f(x,y,z) = \cos(\omega x)\cos(\omega y)\cos(\omega z) - \sin(\omega x)\sin(\omega y)\sin(\omega z) \qquad (2.7)$$

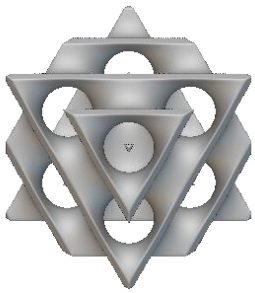

Figure 2.3: *Visual Representation of the Diamond structure*

iv. **Neovius**

$$3 \cdot (\cos(\omega x) + \cos(\omega y) + \cos(\omega z)) + 4\cos(\omega x)\cos(\omega y)\cos(\omega z) \qquad (2.8)$$

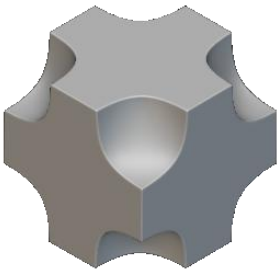

Figure 2.4: *Visual Representation of the Neovius structure*

These representations also highlight the differences between surface types. For example, the Gyroid, has no straight lines or planar symmetries, making it structurally robust and isotropic. The Primitive and Diamond surfaces, by contrast, have more regular repeating patterns and distinct Bonnet angles, with the Primitive defined at 90°, the Diamond at 0°, and the Gyroid at 38.014°.

3. **Numerical Minimization of Surface Energy**:

This is often carried out using specialized computational tools such as Surface Evolver, a program created by Ken Brakke for studying surfaces governed by energies such as surface tension, gravity, and contact forces. In this approach, TPMS are modeled as area-minimizing surfaces. Since every point on a minimal surface is a saddle point, TPMS are inherently unstable and must be carefully defined under constraints. The mean curvature of a surface is given as:

$$H=\frac{k_1+k_2}{2} \tag{2.9}$$

where k_1 and k_2 are the principal curvatures in orthogonal directions. The energy functional is defined as the integral of the squared mean curvature:

$$\int (H-H_0)^2 \, dS = 0 \tag{2.10}$$

where H_0 is the target mean curvature, often set to zero for minimal surfaces. At equilibrium, this energy reaches its minimum, producing a stable representation of the surface. In theory, one can always redefine the square of the gradient of the original energy as a new energy functional, which is minimized at equilibrium states of the original system.

2.7. ADVANCES IN TPMS HEAT EXCHANGER RESEARCH

Traditionally, research has concentrated on three canonical structures, Gyroid (G), Diamond (D), and Primitive (P) characterized by uniform porosity and periodicity. While effective, these geometries lack inherent directional flow control or variable porosity features. Recent work has broadened the TPMS design space: Rathore et al. (2022) compared G, D, P, and I-WP; Wang et al. (2024) experimentally tested seven geometries, including Neovius and Fischer-Koch S; and Barakat and Sun (2024) introduced new sheet-TPMS geometries that exceeded Gyroid and Diamond by up to 27.2% and 18% in thermal performance. Novel forms such as G-Prime and FRD (Kwasi-Effah et al., 2024) achieved up to 70% higher thermal energy density than Schwarz-Diamond, with improved j/f ratios, underscoring the potential of hybridized geometries.

Recent advances have focused on tailoring TPMS morphology to optimize heat transfer and flow resistance. Structural control strategies include gradient wall thickness (Novak,

2022) and hybridized TPMS integrations (Ding et al., 2023), wall thickness or porosity variation, local geometric scaling, surface perforation, recursive or fractal construction, and precise lattice surface shaping (Tang et al., 2024). For example, perforated Gyroid structures achieved 97–366% increases in Nusselt number while reducing pressure drops (Asif, 2022), whereas fractal TPMS exhibited flow resistance trade-offs depending on fractal order (Beer, 2024). Building on this, Zhang et al. (2025) employed the Field Synergy Principle, a concept in convective heat transfer optimization, originally proposed by Guo et al. (1998), that explains how the alignment of velocity and temperature (or scalar) fields can improve heat transfer performance without necessarily increasing energy consumption, to develop a Gradient-Gyroid design, yielding a 6.6% increase in Nusselt number and a 63.1% improvement in overall thermo-fluid performance, demonstrating the promise of gradient optimization.

Parallel studies have emphasized the tunability of TPMS structures. Ibhadode (2024) showed that Gyroid and Diamond lattices can undergo anisotropic deformation to achieve adaptive thermal and mechanical responses. Key performance metrics such as tortuosity, surface connectivity, wall thickness, and curvature distribution strongly influence cooling efficiency and energy absorption (Yeranee & Rao, 2022; Lyu et al., 2024). Collectively, these innovations establish TPMS not only as efficient heat exchangers but also as tunable, multifunctional architectures adaptable to diverse operating conditions.

A major research opportunity lies in creating a standardized evaluation framework that permits side-by-side comparison of TPMS forms under commercial operating conditions, including variable thermal gradients, real-time fouling, and system-level integration effects.

2.8. ADDITIVE MANUFACTURING (AM)

Additive Manufacturing (AM), also referred to as Rapid Prototyping (RP), is defined by ASTM F2792-10e1 as "the process of joining materials to make objects from 3D model data, usually layer upon layer, as opposed to subtractive manufacturing methodologies, such as traditional machining". This method facilitates the creation of highly intricate geometries directly from digital files, offering reduced lead times and enabling the fabrication of structures previously considered unmanufacturable (Kumar et al., 2022). Additive manufacturing broadly falls into three different categories based

on the state of the print material. These are filament deposition, sintering (powder) and light (resin) (Hawken et al., 2023).

Modern AM techniques offer a versatile platform for engineering highly complex heat exchanger cores, particularly those utilizing triply periodic minimal surface (TPMS) geometries. These structures benefit from AM's capacity to produce intricate curvatures, internal channels, and smooth surface transitions without the need for extensive tooling. Among the leading AM technologies, Laser Powder Bed Fusion (L-PBF) has emerged as a frontrunner for metal-based TPMS fabrication due to its fine resolution and structural fidelity (Careri et al., 2023; King et al., 2015).

Surface finishing methods such as electrochemical polishing, chemical etching, and annealing are increasingly applied to AM TPMS cores to enhance thermal reliability, flow uniformity, and fouling resistance. Roughness strongly influences heat transfer and fouling, with higher roughness contributing to pressure drop (Herz et al., 2023). Yan et al. observed that significant surface roughness not only increases flow resistance and disrupts flow uniformity, but also lead to localized blockages. Thus, TPMS performance depends as much on post-processing and material behavior as on geometry.

2.9. REVIEW OF PREVIOUS STUDIES ON TPMS HEAT EXCHANGER DESIGN AND ANALYSIS

Yan et al. (2023) numerically investigated TPMS-structured heat exchangers with uniform unit cell size and wall thickness, comparing Diamond, Primitive, Gyroid, and IWP geometries against latticework and printed circuit heat exchangers (PCHEs). The Diamond, Gyroid, and IWP demonstrated superior thermal-hydraulic behaviour, with 90–110% PEC improvement over PCHEs within Reynolds numbers of 200–500, while clearly surpassing latticework HXs. The Primitive structure, though regular in flow, showed weaker performance. Diamond achieved the best volumetric efficiency, while Gyroid offered higher gravimetric performance. Flow analysis highlighted geometry-dependent effects: Gyroid induced secondary helical circulation enhancing local convective transfer, Diamond displayed dominant helical motion, and IWP followed sinusoidal merge-split paths, facilitating homogenization of mass, momentum, and energy. Consequently, TPMS-HXs were classified as “three-dimensional homogeneous

mixing flow heat exchangers". Mixing performance generally increased with Reynolds number, though IWP-hot showed a minimum at Re = 450. At 0.01 kg/s, mixing ranked Diamond > Gyroid > IWP-hot > IWP-cold.

Tang et al. (2023) discovered that within the Reynolds number range of 166-943, the Nusselt number of the Diamond-type TPMS was 1.16-1.28 times greater than that of the Gyroid. In the direction of flow, the Diamond structure lacks "through- hole" structures, while the Gyroid has a larger "through-hole" area. This "through-hole" structure may weaken fluid mixing, leading to weaker convective heat transfer performance in the Gyroid when compared to the Diamond. Therefore, reducing the "through-hole" in the Gyroid may enhance fluid mixing, thus strengthening convective heat transfer.

Peng et al. (2019) benchmarked a Gyroid TPMS-based heat exchanger against a traditional plate heat exchanger with identical dimensions, demonstrating remarkable thermal advantages. The TPMS heat exchanger exhibited substantially larger interfacial surface area, enabling heat transfer rates up to 7.5 times higher and heat transfer coefficients enhanced by nearly 88.5%. Mixing-cup outlet temperatures showed much closer hot–cold convergence, confirming superior thermal exchange. However, this enhancement was accompanied by higher pressure drops, reaching 19.15 Pa at 20 mm/s compared to only 1 Pa in the reference exchanger. An industrial-size TPMS-HX was printed with an EOS M290 DMLS machine but unfortunately, the Gyroid heat exchanger with a uniform wall thickness of 0.2 mm failed due to leakage problem encountered during the manufacturing stage. A manufacturability study on the TPMS-HX showed that a wall thickness larger than 0.2 mm was desired.

Kus et al. (2024) fabricated and experimentally validated a gyroid-based AM heat exchanger, showing that despite being 30% smaller in volume than a reference plate heat exchanger, the AM device achieved on average 10.5% higher number of transfer units (NTU) and 5% greater temperature effectiveness, though with an ~18% higher pressure drop.

Röver et al. (2023) demonstrated that an additively manufactured Schwarz diamond TPMS exchanger achieved 108% higher compactness and 54% lower weight compared to a conventional plate heat exchanger, while simultaneously reducing pressure losses by 50–59% and modestly improving heat transfer by 3–5%. These works highlight the

design freedoms enabled by AM, such as the integration of TPMS structures and tailored flow paths, not achievable with brazed-plate or tube-fin designs, thereby offering superior performance-to-weight ratios. However, they also reveal the trade-off between enhanced compactness and increased hydraulic resistance, underscoring the need for optimization strategies to balance thermal effectiveness and pumping power.

Attarzadeh et al. (2022) compared the thermal efficiency and pressure drop of gyroid, Diamond, and Primitive structures under laminar and transitional flow regimes. Their simulations indicated that gyroid exhibited the most uniform temperature distribution but incurred higher pressure losses due to its more tortuous channels.

Brambati et al. (2024) developed a unified heat transfer correlation capable of predicting the convective heat transfer coefficient across different TPMS topologies (Gyroid, Schwarz-Primitive, and Schwarz-Diamond) under fully turbulent flow conditions (Re = 5,000–50,000), for fluids with Prandtl numbers between 0.7 and 7, and for varying unit cell sizes and porosities. Their study highlighted the role of viscous work terms, with the Schwarz-Primitive geometry showing the strongest sensitivity to this effect. The proposed correlation was benchmarked against traditional formulations, which were found to significantly underestimate heat transfer in TPMS-based exchangers, as well as against existing TPMS-specific correlations, confirming its superior predictive accuracy relative to CFD results. Additionally, a modified version incorporating total rather than static temperature was introduced, yielding better agreement in high-speed flow regimes.

Efforts to broaden correlation generality included Kus et al. (2024), who integrated both Reynolds and Prandtl numbers into their formulations, following the canonical $Pr^{1/3}$ scaling from heat transfer theory. Though limited to a single porosity case, their work represented an attempt to expand predictive frameworks across different fluids with varying thermal properties. Baobaid et al. (2022) evaluated free convection in TPMS heat sinks, producing empirical Nusselt–Rayleigh relationships for Diamond-Solid, Gyroid-Solid, and Gyroid-Sheet morphologies. Collectively, these correlation studies underscore the predictability of TPMS enhancements, but they also reveal strong dependencies on porosity, topology, and operating flow regime. The lack of comprehensive datasets covering wide porosity ranges, multiple fluids, and extended

Reynolds numbers restricts the robustness of existing models and motivates future systematic explorations.

Numerical modeling has remained the dominant tool for investigating TPMS heat exchangers, largely due to the complexity of fabricating intricate geometries and the difficulty of experimental measurement at high temperature and pressure. A wide range of numerical strategies has been employed, each with trade-offs in accuracy, computational cost, and scalability. Body-fitted CFD based on finite volume or finite element methods has historically been the most common, as it allows precise representation of TPMS geometries and accurate resolution of conjugate heat transfer.

Attarzadeh et al. (2021) applied this approach to Diamond TPMS under laminar conditions, revealing significantly higher Nusselt numbers than stochastic foams. Iyer et al. (2022) extended these methods across laminar and turbulent regimes, producing performance correlations that remain widely cited. Fu et al. (2019) constructed a counterflow TPMS heat exchanger model using CFD, demonstrating that gyroid geometries provided superior performance at moderate Reynolds numbers. These works collectively validated the high-performance potential of TPMS structures but also highlighted the computational burden of meshing thin-walled geometries. In response to meshing difficulties, voxelation and Cartesian-grid approaches have emerged as alternatives.

Jiang et al. (2021) used voxel-based method to adaptively generate and optimize functionally graded TPMS. While voxelation introduces errors at solid–fluid interfaces, advances in adaptive refinement have improved accuracy, making this approach increasingly viable for comparative studies.

Unit-cell homogenization has been another influential method, where researchers simulate periodic boundary conditions on a single TPMS unit cell to extract effective transport properties. Saghir et al. employed a Darcy–Brinkman framework to compare gyroid with metal foams, demonstrating superior heat transfer. Piedra et al. (2023) similarly studied Primitive and I-WP unit cells, finding pressure behavior that aligned with Darcy–Forchheimer scaling. Attarzadeh et al. (2021) and Iyer et al. (2022) also relied on homogenized unit cells to produce Nusselt–Re correlations, which are particularly valuable for scaling up to system-level designs. The efficiency of

homogenization enables wide parametric sweeps, but the reliance on periodic assumptions omits entrance, exit, and maldistribution effects that are critical for real exchangers. Alternative methods such as the lattice Boltzmann method (LBM) have also gained traction.

Reynolds et al. (2023) applied LBM to gyroid TPMS, reporting maximum heat transfer rates under optimal conditions, while Luo et al. used LBM to compute diffusivity, conductivity, and tortuosity. LBM is particularly suited to TPMS geometries due to its voxel-based grid structure and scalability on GPUs, though it is limited to low Mach number flows. Nevertheless, the rise of computational resources positions LBM as a powerful future tool for TPMS research.

These numerical methods, validated through extensive benchmarking, now offer designers the ability to screen thousands of TPMS variants across loading, flow, and thermal conditions.

2.10. SUMMARY OF FINDINGS IN LITERATURE

The literature on TPMS-based heat exchangers reveals significant progress in understanding the thermal and mechanical behaviour of elementary lattice structures; however, research has largely remained confined to unit-cell scale analyses rather than full device performance. While numerous studies report heat transfer and pressure drop characteristics, only a few address second-law metrics such as exergy destruction, which are crucial for assessing real system efficiency. Moreover, investigations into advanced working fluids remain limited, with almost no studies incorporating oils or liquid metals despite their industrial relevance.

A major gap lies in the absence of standardized benchmarking frameworks across TPMS geometries, without consistent test conditions or comparative datasets, selecting optimal structures remains an ad hoc process. Emerging evidence suggests that heat transfer outcomes are governed more strongly by the interplay between flow regimes and internal geometries than by global parameters like porosity or surface area, highlighting the need for flow-geometry coupled design approaches. Current research also tends to overlook process integration, sustainability considerations, and long-term durability. Issues such as embodied energy in additive manufacturing, material recyclability, fouling resistance, and fatigue under cyclic loading remain

underexplored. It could not also be determined through research which TPMS geometry is most suitable for heat exchanger applications. Collectively, the findings are intended to guide future experimental work, inform manufacturable design constraints, and support the broader adoption of TPMS structures in high-efficiency heat exchangers.

CHAPTER 3

METHODOLOGY

This chapter describes the computational framework and simulation strategies employed to analyze the overall performance and flow characteristics of the full-scale TPMS heat exchanger. The methodology refers to a complete heat exchanger assembly model, including all flow channels, solid walls, and boundaries, to accurately represent the system's real-world behavior. This approach allows for the comprehensive evaluation of system-level metrics, such as total pressure drop across the device, thermal effectiveness, and local heat transfer variations.

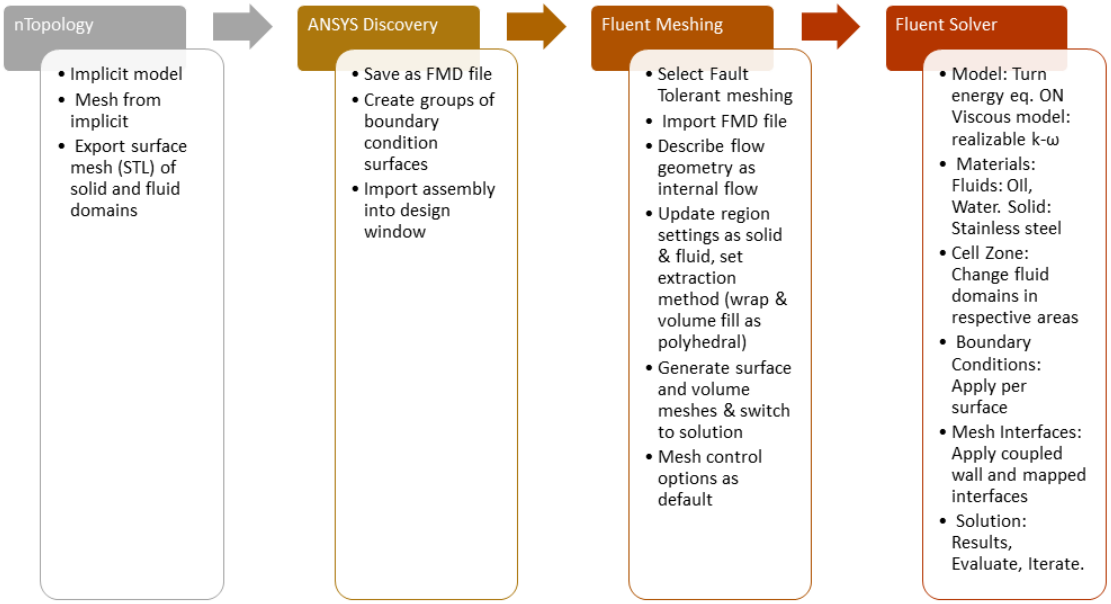

Figure 3.1: *Methodology process flowchart*

3.1. DESIGN AND CHARACTERIZATION OF TPMS HEAT EXCHANGERS

The investigation adhered to the structured workflow presented in the guiding framework. This process was carefully developed and grounded in standard CFD analysis methodologies, providing a reliable and repeatable framework for accurately modelling and analysing thermo-hydraulic behaviour of TPMS Heat Exchangers.

Designing a TPMS heat exchanger requires balancing of key factors that affect thermal performance, hydraulic efficiency, and manufacturability. The primary factors include:

1. **TPMS Type:**

The choice of structure (e.g., Gyroid, Diamond, Primitive) dictates the core's surface area density, curvature, and strut connectivity, which are the primary drivers of flow mixing and heat transfer. Complex topologies, due to their large surface-to-volume ratios and zero mean curvature, significantly enlarge the effective heat transfer area.

2. **Wall Thickness:**

This parameter is a critical trade-off between thermal resistance and manufacturability. While a thinner wall minimizes thermal resistance, manufacturing studies on AM processes indicate that a wall thickness larger than 0.2 mm; necessary to ensure successful fabrication and prevent leakage, thereby fulfilling structural integrity requirements.

3. **Unit Cell Size**

The characteristic length of the repeating lattice structure directly controls the size of the flow channels. Reducing the unit cell size enhances convection by thinning the boundary layers but leads to a significant rise in pressure drop and weight of the HX unit.

4. **Domain Bias**

The Domain bias is the size of one of the domains to the other. The bias contracts or expands one domain relative to another and when the bias is zero, the interpenetrating domains of TPMS are equally divided in the 3D volume. For a TPMS with a bias greater than or less than zero, one fluid domain will expand, and the other will contract. The bias is useful in the consideration of heat transfer efficiency and hydrodynamic resistance of flowing fluids and thus, can be adjusted for design optimization.

The design strategy focused on selecting a TPMS structure that achieved the best balance between high thermal performance and structural viability. Among the leading options, structures like the Diamond often show the highest local convective performance due to intense wall-fluid interactions. However, the Gyroid TPMS was ultimately selected as the optimum core geometry for this investigation. This decision was based on its demonstrated superior overall performance metrics from having smooth, interconnected channels that are highly effective at inducing a secondary helical circulation which facilitates the homogenization of momentum, mass, and energy, thereby strengthening convective heat transfer while providing strong structural properties.

3.2. COMPUTATIONAL MODELLING

Traditional Boundary-representation (B-rep) CAD platforms struggle computationally with intricate TPMS structures, as file size and processing requirements increase exponentially with geometric complexity. nTopology known as nTop, implements implicit modelling as its core framework, defining geometry through continuous mathematical functions rather than discrete boundary elements, thereby, enabling the direct construction of complex lattices while minimizing computational cost. Its mathematically robust framework allows Boolean operations which creates error-free, full-scale domains as a single part. The entire process is captured in a reusable and repeatable workflow of nTop Blocks, creating a non-destructive, configurable design ideal for rapid iteration. These features make nTop particularly suited for advanced heat exchanger design and justifies its adoption in this research.

3.2.1. GEOMETRY DESIGN

The modelling workflow in nTopology followed a structured, five-phase approach encompassing the definition of the external envelope, creation of the internal TPMS core and fluid domains, integration of hydraulic optimization features, final assembly and encapsulation, and meshing.

1. **External envelope definition:**

A Box primitive established the external form factor, with its length, width, and height serving as key input parameters that set the bounding volume for subsequent operations. A Smoothen Body block was first applied to round sharp edges. This box was shelled to a defined thickness to form the outer casing, providing structural and thermal containment. Cylinder primitives were then created for the inlet and outlet ports, their positions parametrically linked to the box corners to maintain alignment during dimensional changes. Boolean operations unified the ports with the shell, pierced openings for the pipes, and applied fillets at the fluid entry points to improve flow and reduce pressure drop, completing the external geometry setup.

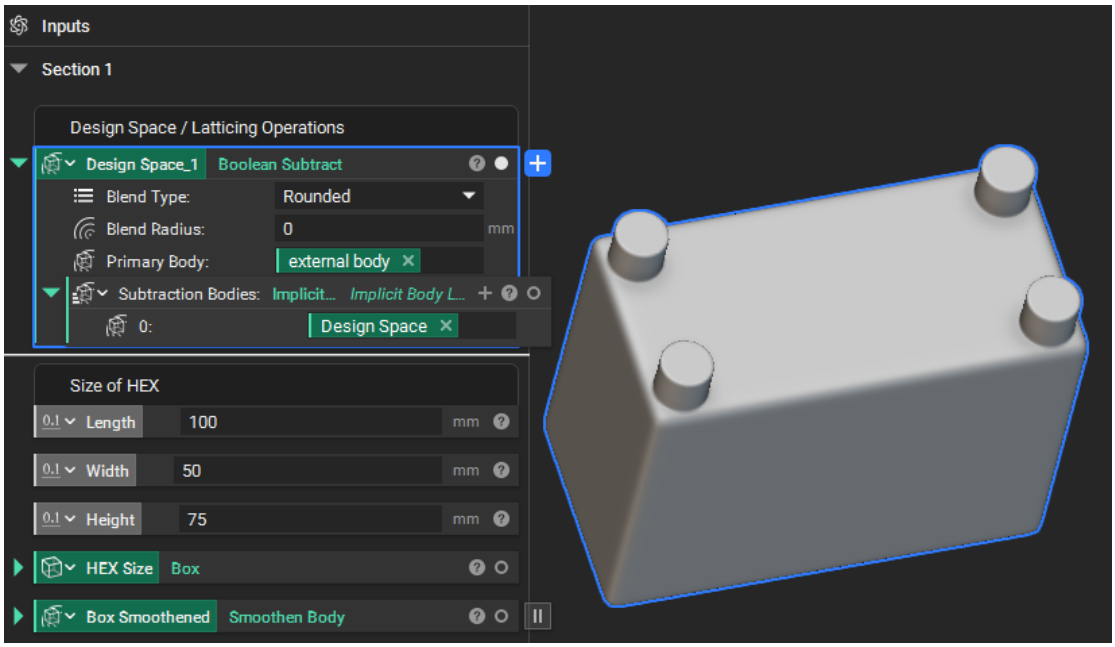

Figure 3.2: *External geometry setup*

2. **Internal Core Generation:**

This internal core was infilled with a Gyroid lattice. The generation of these domains was controlled by two key variables: Cell Size and Wall Thickness. The workflow segregated the internal volume into three distinct, non-intersecting implicit bodies. First, a Walled TPMS block was used to generate the solid heat exchanger wall. Second, a separate TPMS block, using identical parameters, was created to represent the volume of the first fluid. Finally, the second fluid domain was isolated using a Boolean Subtraction, removing both the Walled TPMS and Fluid Domain 1 from the original bounding volume.

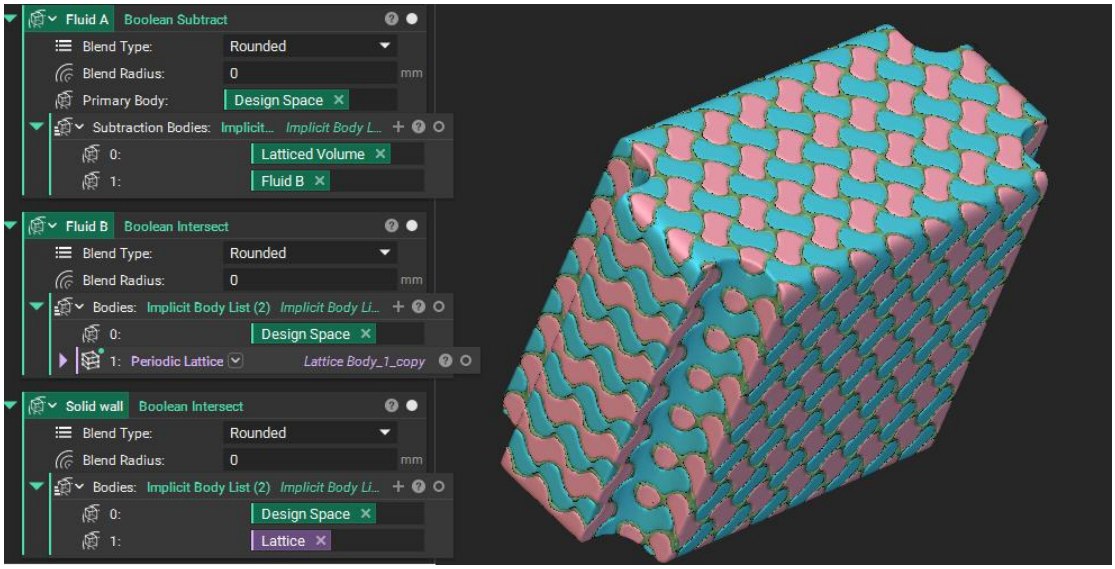

Figure 3.3: *Internal Core generation*

3. **Generation of Functional Interfaces:**

A significant challenge in TPMS heat exchangers is ensuring the two fluid domains remain separate at the inlets and outlets. To solve this, internal baffles were designed. Cylinder primitives, co-located with the main ports, were thickened to act as plugs. Through Boolean operations, these baffles were integrated with the Gyroid core to precisely intersect and block the entrance to the opposing fluid's domain, guaranteeing a fully sealed separation.

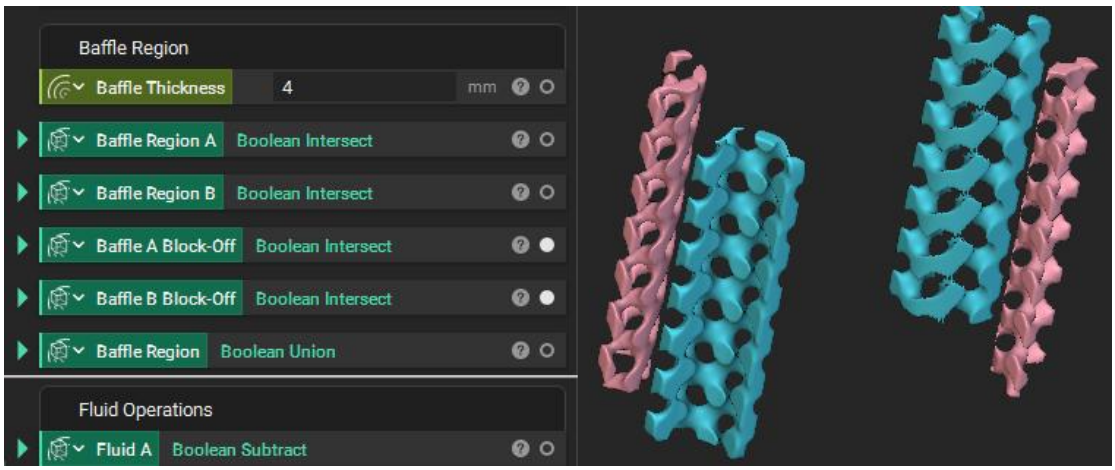

Figure 3.4: *Baffles*

4. **Model Assembly:**

The final modelling step involved assembling all discrete implicit components. A Boolean Union operation was performed to combine all geometric elements: the shelled outer casing, the inlet/outlet pipes, and the complex, baffled Gyroid core. This results in a single, contiguous, and manifold solid model. The most powerful step in the methodology was the encapsulation of this entire sequential process into a single, reusable custom block. The key design variables, such as Length, Width, Shell Thickness, Cell Size, and Wall Thickness, were exposed as the primary inputs for this new, consolidated block.

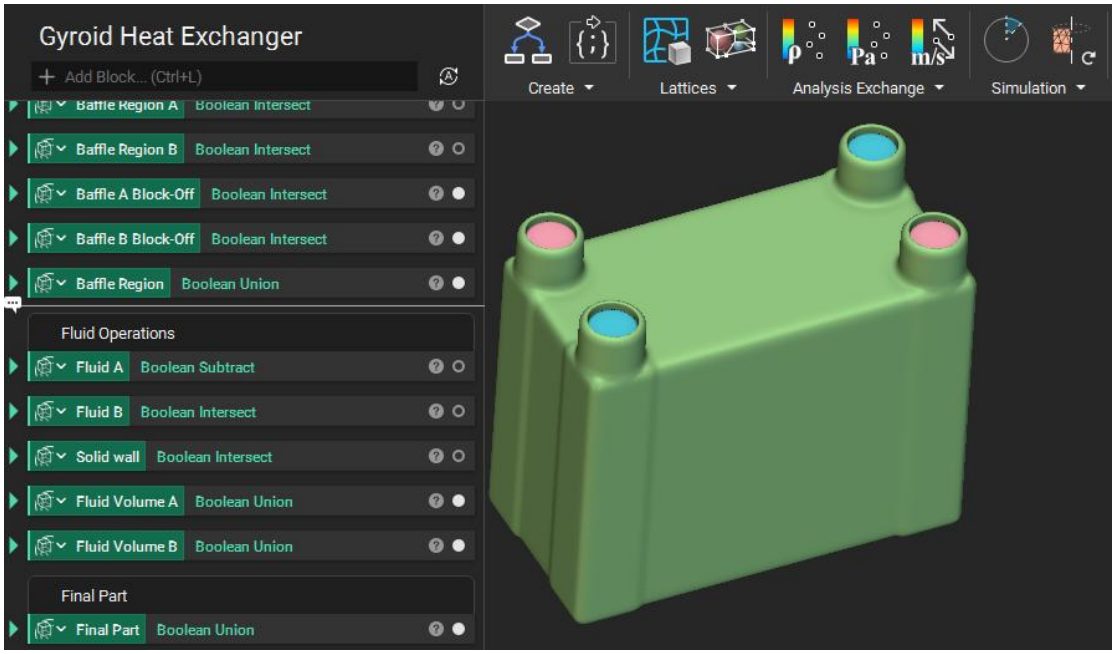

Figure 3.5: *Assembled Heat Exchanger model*

5. **Export Surface Mesh for CFD**

Finally, the implicit geometry was converted into a high-quality surface mesh. The meshing process involved a two-step refinement: initially, the Mesh from Implicit Body block produced a fine, high-element-count mesh. This was followed by the Remesh Surface operation, applied to ensure high-quality elements while preserving sharp features. The final, high-quality surface meshes for the hot, cold, and solid domains were then exported as .STL files.

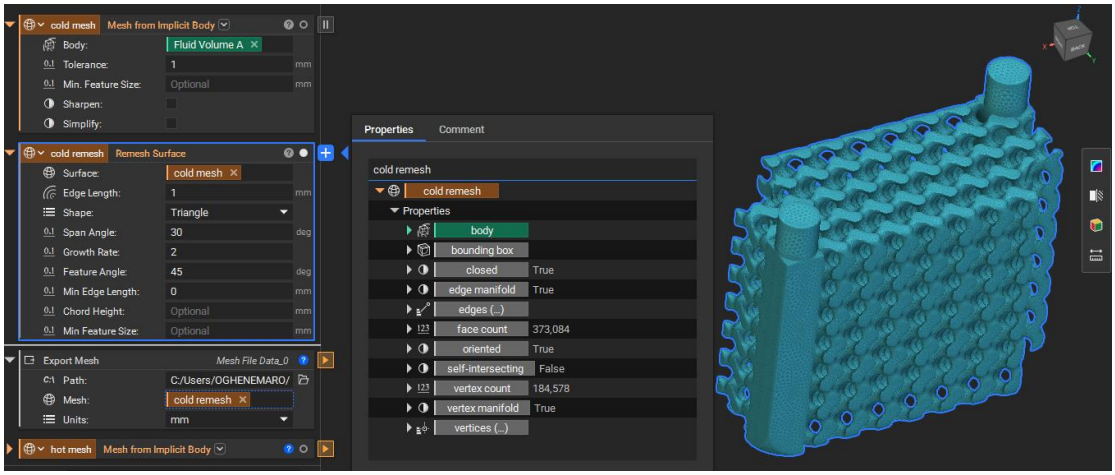

Figure 3.6: *Cold Surface Mesh and Export*

3.2.2. GEOMETRIC PROPERTIES OF TPMS HEAT EXCHANGERS

A rigorous non-dimensional analysis begins with the choice of physically meaningful lengths. In TPMS geometries the presence of multiple geometric scales; unit-cell size, wall thickness, and the wetted surface area per unit volume, makes this choice non-trivial.

ϕ is the porosity of the TPMS structure defined as the fluid volume fraction, given by;

$$\phi = \frac{V_{\text{fluid}}}{V_{\text{total}}} \tag{3.1}$$

The specific interfacial area a_{sf} is an intrinsic geometric quantity that links microstructure to macroscopic transfer. It is defined as;

$$a_{sf} = \frac{A_{fs}}{V_{\text{cell}}} \ [m^{-1}] \tag{3.2}$$

where A_{fs} (m ^{2}) is the total fluid–solid interfacial area given by:

$$A_{sf} = \iint \sqrt{1 + \left(\frac{\partial z}{\partial x}\right)^2 + \left(\frac{\partial z}{\partial y}\right)^2}\, dx\, dy \tag{3.3}$$

contained in the chosen reference volume V_{cell} (m ^{3}), typically taken as one TPMS unit cell or an integer multiple thereof.

The specific interfacial area a_{sf} is calculated from the mesh-derived surface area of the TPMS core structures generated in nTop. Reporting a_{sf} allows comparison of surface availability for convection; how much heat-exchange surface sits inside one cubic centimeter of a given TPMS topology. The concept of specific interfacial area is standard in porous media and porous-type heat-transfer analysis (Whitaker, 1999).

From a_{sf} and porosity ϕ one may define a bulk TPMS hydraulic diameter that is consistent with the usual hydraulic diameter in ducts but that reflects porous geometry:

$$D_{\text{h}}=\frac{4\phi}{a_{sf}} \quad [m] \tag{3.4}$$

This form comes from the general definition;

$$D_{\text{h}}=4V_f/A_s \tag{3.5}$$

Where;

V_f = reference volume

A_s= corresponding wetted surface.

Using D_{h} defined this way is advantageous when comparing topologies with different surface densities because it ties the reference scale directly to the volume-averaged fluid geometry rather than to an arbitrarily chosen unit-cell side length (Kays & London, 1984; Whitaker, 1999).

Table 3.1: *Extracted Geometrical Data*

PROPERTY	SYMBOL	FORMULA	VALUE
Design space volume [mm^3]	V_{total}	-	452,947.27

Wall volume [mm^3]	V_{wall}	-	137,036.28
Fluids volume [mm^3]	V_{fluid}	-	315,909.999
Total solid - fluid interaction area [mm^2]	A_{sf}	-	220,781.963
Specific solid- fluid interaction area [mm^{-1}]	a_{sf}	$a_{sf} = \frac{A_{sf}}{V_{\text{total}}}$	0.487434
Porosity	ϕ	$\phi = \frac{V_{\text{fluid}}}{V_{\text{total}}}$	0.697454
Hydraulic diameter [mm]	D_{h}	$D_{\text{h}} = \frac{4\phi}{a_{sf}}$	5.72347

3.3. NUMERICAL MODELING

The complexity of the geometries investigated necessitates the use of a CFD tool capable of handling highly intricate microstructures. ANSYS Fluent is therefore selected as the primary software platform for the numerical analyses presented in this paper. A decisive advantage of Fluent is its incorporation of a dedicated Fault-Tolerant Meshing (FTM) workflow. This specialized template is crucial for effectively discretizing rough, implicitly-modeled structures, such as the TPMS topologies investigated in this work. The FTM capability significantly streamlines the pre-processing phase by efficiently generating high-quality volume meshes directly from complex, non-ideal CAD inputs, bypassing the traditional, time-consuming requirement for manual CAD repair.

3.3.1. GOVERNING EQUATIONS

For this work, the mathematical model was developed using the conjugate heat transfer (CHT) approach, which accounts for the interaction between fluid and solid regions through their adjoining boundaries. This framework ensures that the coupled thermal transport across solid walls and fluid domains is resolved in a consistent manner. The fluid flow is governed by the continuity equation and the momentum conservation equation. For a single-phase flow, the general form of the continuity equation is given as;

$$\frac{\partial \rho}{\partial t} + \nabla \cdot (\rho \vec{v}) = 0 \quad (3.6)$$

Where;

ρ = fluid density

$\vec{v}$ = velocity vector

Under the assumption of steady and incompressible flow the equation reduces to;

$$\nabla \cdot \vec{v} = 0 \quad (3.7)$$

The momentum transport was modeled using the incompressible and steady-state form of the Reynolds Averaged Navier-Stokes (RANS) equations;

$$\nabla \cdot (\rho \vec{v} \vec{v}) = -\nabla p + \nabla \cdot [(\mu + \mu_t)\nabla \vec{v}] \quad (3.8)$$

Where;

μ = viscosity

μ_t = turbulent eddy viscosity

3.3.2. TURBULENCE MODELING

Turbulence is one of the most complex aspects of fluid dynamics due to its chaotic behaviour and wide range of interacting eddy scales. Direct Numerical Simulation (DNS) of all turbulence scales is computationally infeasible for high Reynolds number flows commonly encountered in engineering. Hence, turbulence models are adopted to provide reasonable approximations while remaining computationally efficient.

The k- ω Shear Stress Transport (SST) model, developed by Menter (1994), is a widely used two-equation RANS-based model. It blends the near-wall accuracy of the standard k-ω model with the accuracy of the k-ε model in free shear regions. This hybrid approach allows the SST model to better handle flows with strong adverse pressure gradients, flow separation, and complex boundary-layer interactions.

The transport equation for k is;

$$\nabla \cdot (\rho \vec{v} k) = P_k - \beta * \rho k \omega + \nabla \cdot [(\mu + \sigma_k \mu_t) \nabla k] \quad (3.9)$$

while the dissipation rate is governed by;

$$\nabla \cdot (\rho \vec{v} \omega) = \alpha \left(\frac{\omega}{k}\right) P_k - \beta \rho \omega^2 + \nabla \cdot [(\mu + \sigma \omega \mu_t) \nabla \omega] + 2(1 - F_1) \rho \sigma_{\omega 2} \left(\frac{1}{\omega}\right) \nabla k : \nabla \omega \quad (3.10)$$

Here, α, β, and $\sigma_{\omega 2}$ are model constants, and F_1 is a blending function that transitions between the k-ω and k-ε formulations. This hybrid formulation ensures accurate predictions of boundary layer behavior, separation, and recirculation zones. which are critical in conjugate heat transfer problems.

For the energy equations, heat transfer in the fluid region is expressed in terms of specific enthalpy, *h*;

$$\nabla \cdot (\rho h \vec{v}) = \nabla \cdot \left[\left(\frac{\lambda_{eff}}{C_p}\right) \nabla h\right] \quad (3.11)$$

Where;

λ_{eff} = effective thermal conductivity.

C_p = specific heat capacity (kJ/Kg.K)

It is defined as;

$$0 = \nabla \cdot (\lambda \nabla T) \quad (3.12)$$

3.3.3. PRE-PROCESSING

3.3.3.1. GEOMETRY PREPARATION

The STL files from nTopology were imported in ANSYS Discovery to prepare the computational model for subsequent meshing and simulation setup. The preparation process involved:

i. **Unit Configuration and Geometry Import:**

The active unit system in ANSYS Discovery was set to millimetre**s**. This ensures the unitless STL file was imported at the correct 1:1 design scale. The STL files were imported as facet bodies representing the solid TPMS structure.

ii. **Facet Integrity Check:**

Geometry errors such as holes, gaps, fold-overs and self-intersections were checked for and corrected to ensure the model was watertight.

iii. **Boundary Naming:**

Relevant surfaces to were assigned boundaries using the Selections Tool in ANSYS Discovery. This included creating logical names for the physics boundaries such as, “hotinlet”,” hotoutlet”, “coldnlet”, “coldoutlet” and the shared heat transfer surfaces named as “hotintf” and “coldintf.”

3.3.3.2. MESH GENERATION

Meshing was performed in ANSYS Fluent Meshing using the Fault-Tolerant Meshing Workflow to discretize the continuous fluid and solid domains into smaller, defined computational elements suitable for numerical analysis. This workflow was specifically selected to handle the inherent complexity of the nTop-generated geometry and ensure a watertight domain.

The fault tolerant meshing workflow applied to the Full-Scale Heat Exchanger involved:

i. **Importing and Geometry Description:**

The geometry preparation for the simulation involved a multi-step process. First, the model was exported from ANSYS Discovery as an FMD (Fluent Meshing Data) file. This file was then imported directly into the ANSYS Fluent Mesher to begin the meshing process. In the Fluent Mesher, the geometry was defined for an internal flow simulation. A key setting in this setup, "large caps and enclosures", was intentionally set to "no". The rationale for this decision was that the fluid domains were already complete; the original nTop model included the necessary enclosures and capping surfaces at the inlets and outlets, making regeneration of these features in Fluent unnecessary.

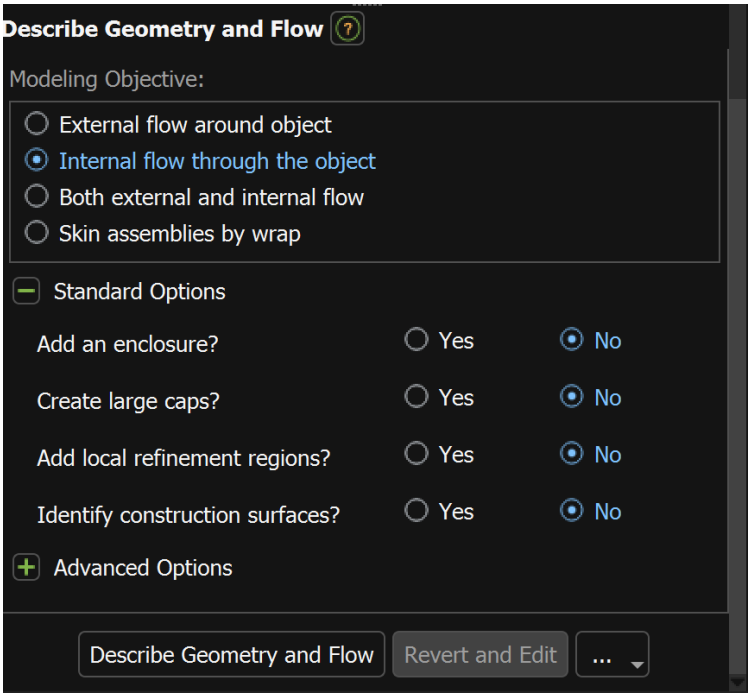

Figure 3.7: *Geometry description*

ii. **Updating the Region Settings:**

Following the geometry import, the simulation domains were defined. The two fluid regions, designated as the "hot domain" and "cold domain," were specified as fluid types. For both of these domains, the volume extraction method was set to WRAP, and the domain was filled with a polyhedral mesh, which balances the benefits of both hexahedral mesh, with its low numerical diffusion and the tetrahedral mesh fast mesh generation. The third body, representing the conductive solid boundaries, was left as the default "solid" type, completing the setup of the distinct physical zones.

iii. **Mesh Control and Generation:**

The default mesh controls in ANSYS were first applied to generate a baseline mesh. Subsequently, the curvature and proximity size functions were activated to vary the mesh size for the grid independence study. The surface mesh was then generated as the first stage of discretization.

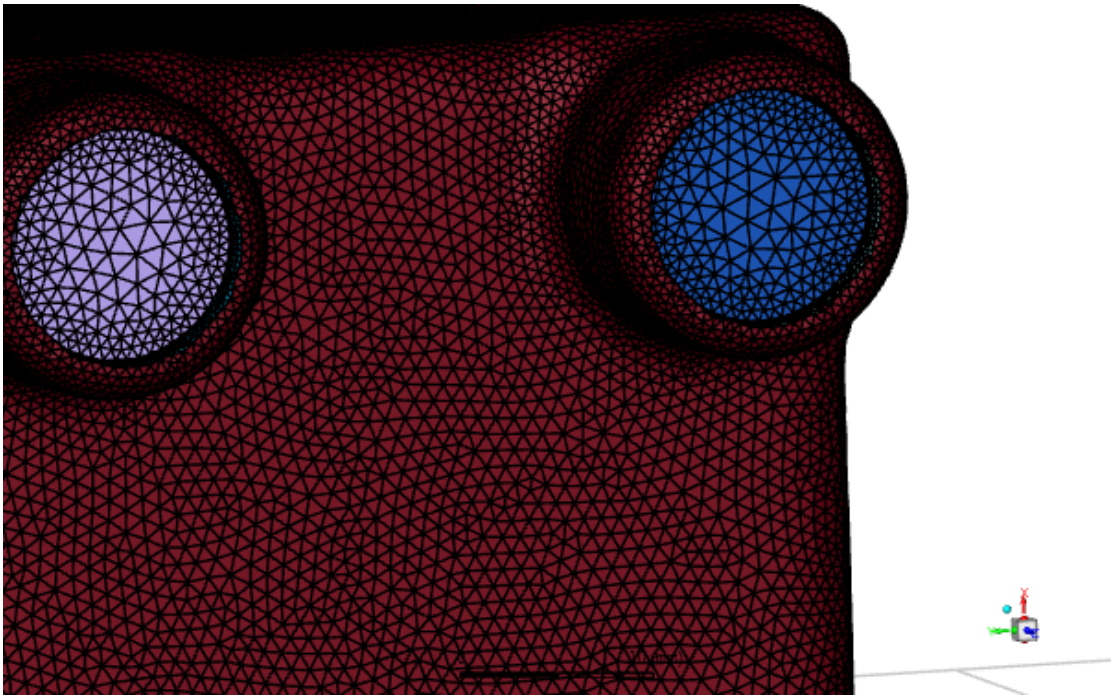

Figure 3.8: *Baseline Mesh of Heat Exchanger Assembly*

iv. **Boundary Layer Addition:**

Boundary layers were introduced on all solid–fluid interfaces. These layers are essential for resolving near-wall gradients in velocity and temperature, which dominate the convective heat-transfer process; 3 inflation layers were generated, starting from the lattice surface with a growth rate of 1.2.

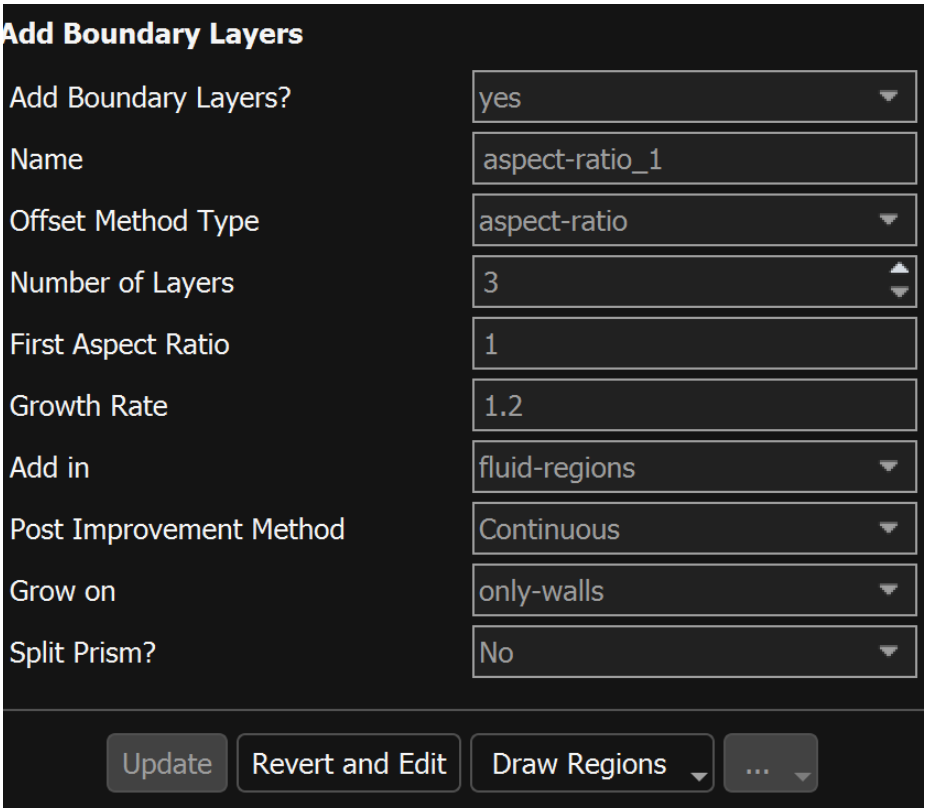

Figure 3.9: *Boundary Layer settings*

v. **Generating the Volume Mesh:**

Following boundary-layer creation, a volume mesh was generated. The fluid and solid region employed polyhedral elements, while prism elements filled the near-wall layers.

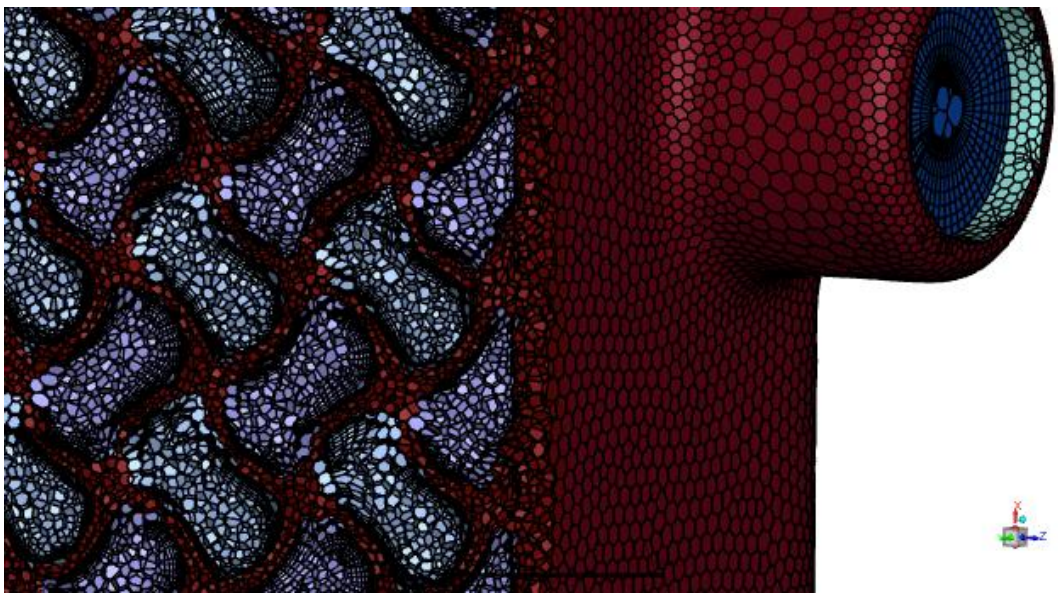

Figure 3.10: *Sectioned view of volume mesh of Heat Exchanger assembly*

3.3.3.3. GRID INDEPENDENCE TEST

The grid independence test ensures that the numerical solution is not significantly influenced by the mesh resolution, thereby validating the accuracy of the simulation results. The grid independence test was carried out using the Richardson extrapolation method. This method involves performing simulations on three systematically refined grids and calculating the GCI using the following equations:

$$R_x = \left(\frac{h_{\text{coarse}}}{h_{\text{fine}}}\right)^{\frac{1}{p}} \tag{3.13}$$

$$p_x = \frac{\ln\left(\frac{f_3 - f_2}{f_2 - f_1}\right)}{\ln(R_x)} \tag{3.14}$$

$$e_{\text{ext}} = \frac{f_3 - f_1}{R_x^p - 1} \tag{3.15}$$

$$GCI_{\text{fine}} = \frac{F_s \times e_{\text{ext}}}{R_x^p - 1} \tag{3.16}$$

Where;

GCI_{fine} = Grid Convergence Index

R_x= refinement ratio

h = the grid spacing,

p_x= observed order of convergence,

$f_{1,2,3}$= solution values on the coarse, medium, and fine grids respectively,

e_{ext} = extrapolated relative error, and;

F_s = safety factor, set to 3 for conservative error estimates.

The grid independence test was performed using the pressure drop across the TPMS structure as the monitored parameter, since it is a key indicator of flow resistance and hydrodynamic performance. Three systematically refined grid levels were tested, and the corresponding pressure drop values were used in the above equations to determine the discretization error and GCI.

3.3.4. PROCESSSING

3.3.4.1. BOUNDARY CONDITIONS AND SOLVER SETUP

The validated computational mesh was imported into the ANSYS Fluent Solver, where the physical phenomena were modeled and simulation parameters were defined

i. **Boundary Conditions**:

The numerical simulation requires specific boundary conditions to define the thermal and fluid interactions at the domain perimeters. The Named Selections previously created in Discovery were assigned the following functional types and values within ANSYS Fluent.

Table 3.2: *Boundary Conditions*

SECTION	SURFACE NAME	BC TYPE	BC PARAMETERS
HOT FLUID	hotinlet	mass flow inlet	mass flow rate = 0.08333kg/s temperature = 350k turbulent intensity = 5% turbulent viscosity ratio = 10
	hotoutlet	pressure outlet	gauge pressure = 0 Pa
	hotwall	wall	adiabatic wall no slip
	hotsolid	wall	no slip
COLD FLUID	coldinlet	mass flow inlet	mass flow rate = 0.08333kg/s temperature = 300k

			turbulent intensity = 5% turbulent viscosity ratio = 10
	coldoutlet	pressure outlet	gauge pressure = 0 Pa
	coldwall	wall	adiabatic wall no slip
	coldsolid	wall	no slip
CORE	solid	wall	adiabatic wall
	solidhot	wall	-
	solidcold	wall	-

ii. **Solver Setup:**

To simplify the simulation heat loss to the environment, viscous heat generation, axial conduction and thermal radiation are neglected. Constant fluid properties were used in the simulations, water has properties that depend on the temperature. Therefore, the properties of the hot and cold side water is taken differently but are constant. Since the inlet and outlet temperatures for hot and cold sides are known, the average temperatures for hot and cold sides are calculated. The fluid properties used in the simulations and experimental calculations are taken at these average temperatures.

The simulation was configured as Steady-State using a Pressure-Based solver, with the Energy Equation enabled to ensure accurate thermal coupling between domains. For turbulence modelling, the k-ω Shear Stress Transport (SST) model was employed. Material properties for the solid core and the fluid were assigned to their respective cell zones. The numerical solution was controlled by the COUPLED algorithm for pressure-velocity coupling, and all governing equations were discretized using the highly accurate Second-Order Upwind scheme. Crucially, the final setup step involved creating Manual Mesh Interfaces between the fluid and solid zones, using the Coupled Wall and Mapped settings to ensure accurate thermal flux transfer across the non-conformal meshes, vital for the integrity of results.

3.3.4.2. SOLUTION PHASE

i. **Report Definitions:**

Mass-weighted averaged outlet velocity, temperature and area-weighted inlet pressure surface reports were defined to specify the values of the computed variables at the end of each solver iteration.

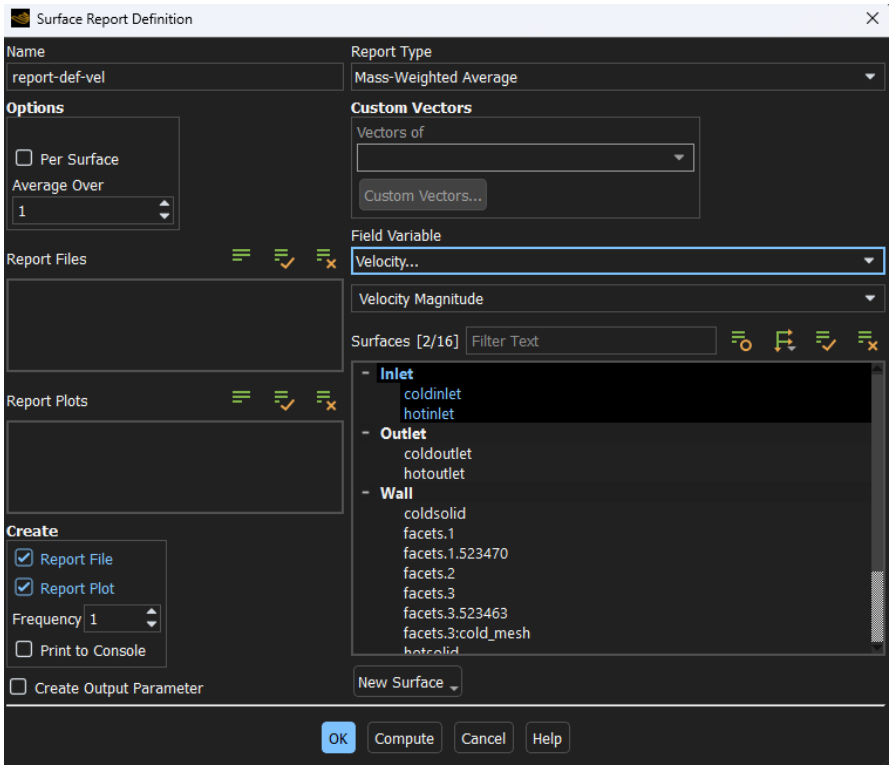

Figure 3.11: *Surface Report Definition*

ii. **Initialization:**

The calculation was initiated using Hybrid Initialization. This method provides a better initial guess for the entire flow field compared to standard methods, which is crucial for complex internal geometries. Hybrid Initialization solves the Laplace equation for velocity and pressure and uses potential flow theory to set an initial starting point for the solver.

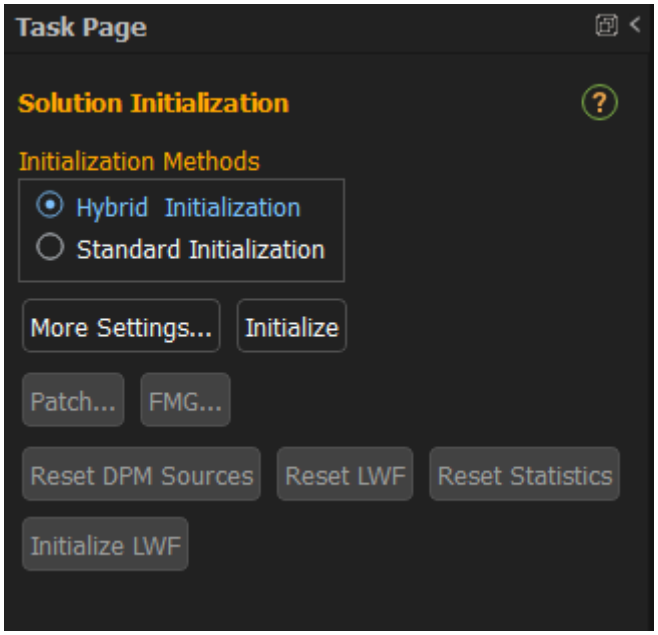

Figure 3.12: *Solution Initialization*

iii. **Convergence Criteria:**

The numerical solution was executed iteratively until stable convergence was achieved. Residual plots were continuously monitored throughout the solving process to confirm that all governing conservation equations satisfied the pre-defined criteria. Upon reaching steady-state convergence, the final flow field, pressure, and temperature distributions were saved as the definitive simulation results for analysis. The CFD solution was considered fully converged based on two criteria for reliable thermal and hydraulic data. Strict Residual Reduction drove residuals to 10^{-1} for continuity, the momentum, and turbulence down to 10^{-3} while the energy equation was held to a stricter threshold of $10^{-6}$for highly accurate heat transfer. Additionally, Global Monitoring Stability confirmed the steady-state by monitoring key performance indicators like the Mass Flux and Interface Heat Transfer Rate, ensuring mass and total energy conservation. The solution was found to converge at 200 iterations.

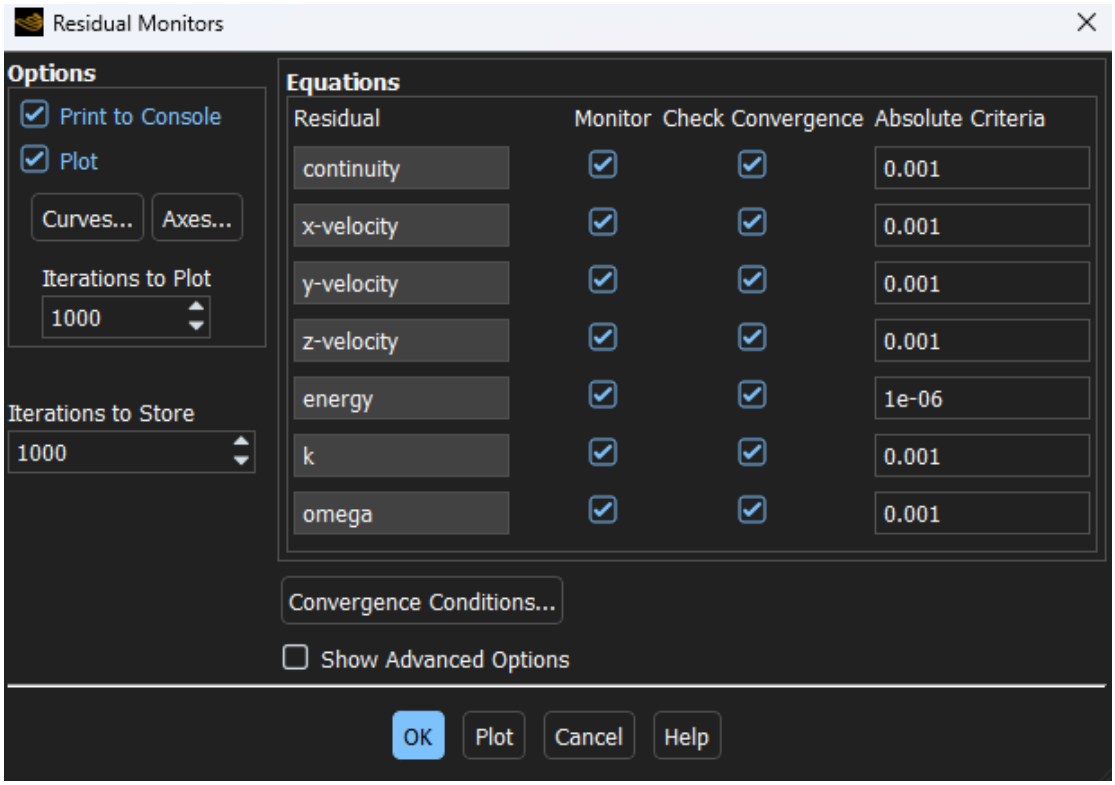

Figure 3.13: *Residual Monitors*

3.3.5. POST PROCESSING

Once a converged solution is achieved in ANSYS Fluent, the simulation results are analyzed using the Report function within ANSYS Fluent. This approach allows direct extraction of key performance parameters without transferring data to ANSYS CFD-Post. In addition to the automated reports, some results were evaluated manually. The calculated flow and thermal data such as velocity, pressure, and temperature distributions are processed to determine standard heat exchanger performance metrics, which are broadly categorized into thermal performance and hydraulic performance.

3.4. THEORETICAL FORMULATIONS FOR HEAT EXCHANGER EVALUATION

3.4.1. FUNDAMENTAL NON-DIMENSIONAL GROUPS

The Reynolds number is defined using the chosen hydraulic diameter and the chosen velocity scale:

$$\mathrm{Re} = \frac{\rho v D_\mathrm{h}}{\mu} \tag{3.17}$$

Where;

ρ = fluid density [kg m $^{-3}$]

μ = dynamic viscosity [Pa·s (kg m $^{-1}$ s $^{-1}$)],

v = selected velocity (m s $^{-1}$), and

D_h = hydraulic diameter (m).

In TPMS contexts authors occasionally compute both $\mathrm{Re}_s=\rho v_s D_\mathrm{h}/\mu$ (superficial definition) and $\mathrm{Re}_p=\rho v_p D_\mathrm{h}/\mu$ (pore/interstitial definition) and they report which is used for fitting correlations.

The Prandtl number is a fluid property ratio of momentum to thermal diffusivity,

$$\mathrm{Pr} = \frac{\mu c_p}{k_f} \tag{3.18}$$

Where;

c_p = fluid specific heat [J kg $^{-1}$ K $^{-1}$] and

k_f = fluid thermal conductivity [W m $^{-1}$ K $^{-1}$].

Pr influences whether thermal boundary layers are thicker or thinner than momentum boundary layers (Incropera & DeWitt, 2011).

The Péclet number combines Reynolds and Prandtl numbers,

$$\mathrm{Pe} = \mathrm{Re}\cdot\mathrm{Pr} = \frac{\rho c_p v D_\mathrm{h}}{k_f} \tag{3.19}$$

and is often used where advection dominates diffusive transport. Pe has units that cancel to dimensionless and is especially useful in scaling convective transport relative to thermal diffusion in TPMS cores.

The Nusselt number Nu is a dimensionless number used in heat transfer to compare convective heat transfer to conductive heat transfer across a fluid boundary layer.

$$Nu = \frac{U D_{\mathrm{h}}}{k_f} \tag{3.20}$$

3.4.2. HYDRAULIC METRICS

Hydraulic metrics quantify the energy cost of flowing a fluid through a TPMS core and are central in any multi-objective optimization that balances heat-transfer gains against pumping penalties. The pressure drop Δp is defined as the difference between inlet and outlet static pressures measured across a specified length L;

$$\Delta p = p_{\mathrm{in}} - p_{\mathrm{out}} \; [Pa] \tag{3.21}$$

Pressure-drop measurements must be accompanied by the exact length L over which they were taken; for periodic channels it is common to report Δp per unit length or to use fully developed periodic boundary conditions in DNS.

The friction factor f in Darcy–Weisbach form is the dimensionless normalization

$$f = \frac{2\,\Delta p\, D_{\mathrm{h}}}{\rho\, v^2\, L} \tag{3.22}$$

where v is the velocity used in the Reynolds number. This friction factor is convenient because it collapses data across different flow speeds and device scales, provided the same D_{h} and v definitions are used. Empirical studies typically present f as a function of Re and fit a power law $f = A\,\mathrm{Re}^{-n}$. At low Re viscous effects dominate and the exponent n may approach 1, whereas at higher Re inertial contributions change the effective exponent, tending towards 2.

Pumping power $\dot{P}$ is the rate of mechanical work required to overcome the pressure drop for a given volumetric flow and is simply

$$\dot{P} = \frac{\dot{V}\Delta p}{\eta_p}[W] \tag{3.23}$$

where $\dot{V}$ is volumetric flow rate [m ^{3} s $^{-1}$].

TPMS topology influences both Nu and f, these hydraulic measurements are indispensable when gauging the real application value of a novel geometry: a geometry that yields a 20% Nu boost at the cost of doubling $\dot{P}$ might be unsuitable for energy-sensitive applications despite its thermal advantage.

3.4.3. COMBINED THERMAL-HYDRAULIC METRICS

To reduce the Nu/f trade-off to a single engineering number, combined metrics are commonly used. The Colburn j-factor is defined as

$$j = \frac{\mathrm{Nu}}{\mathrm{Re}\,\mathrm{Pr}^{1/3}} \tag{3.24}$$

and is widely used in compact heat-exchanger literature because it collapses Nu data across fluids with different Prandtl numbers and provides a normalized heat-transfer indicator independent of fluid choice (Kays & London, 1984). The j-factor is useful when comparing the convective potential of different TPMS topologies for a given hydraulic condition.

The Performance Evaluation Criterion (PEC) is widely used in enhanced-surface literature and in TPMS studies to weigh thermal improvement against hydraulic cost. A common form is

$$\mathrm{PEC} = \frac{(\mathrm{Nu}/\mathrm{Nu}_0)}{(f/f_0)^{1/3}} \tag{3.25}$$

where subscript 0 denotes a chosen reference, which in this study is a straight channel. The baseline friction factor for laminar flow is calculated as:

$$f_0 = \frac{64}{Re} \tag{3.26}$$

The baseline friction factor is calculated using the Petukhov equation:

$$f_0 = (0.790ln(Re) - 1.64)^{-2} \tag{3.27}$$

For laminar flow with a constant heat flux boundary condition, the Nusselt number is a constant:

$$Nu_0 = 4.36$$

Turbulent Flow for turbulent flow the baseline Nusselt number is calculated using the Gnielinski correlation:

$$Nu_0 = \frac{\left((f_0/8)(Re - 1000)Pr\right)}{\left(1 + 12.7(f_0/8)^{0.5}(Pr^{(2/3)} - 1)\right)} \tag{3.28}$$

The exponent 1/3 in the denominator approximates the scaling of pumping power costs with velocity under certain assumptions and therefore weights hydraulic penalty relative to thermal gain; PEC values greater than unity indicate net beneficial performance under the specific weighting.

3.5. HEAT EXCHANGER ANALYSIS

The convective heat-transfer coefficient on either the hot or cold side may be written in terms of the interfacial heat flux and the log-mean temperature difference (LMTD). When q'' denotes the interfacial heat flux ($W \cdot m^{-2}$) across the solid–fluid boundary, the heat-transfer coefficient for side i (where i= h for hot or i= c for cold) is defined as

$$h = \frac{q''}{\Delta T_{LM,i}} \quad [W\ m^{-2}\ K^{-1}] \tag{3.29}$$

where $\Delta T_{\mathrm{LM},i}$ is the log-mean temperature difference for side i. For counter-flow configurations the appropriate LMTD expressions use the bulk inlet and outlet temperatures of the two fluids. For the hot (h) and cold (c) channels the LMTDs are

$$\Delta T_{\mathrm{LM,h}} = \frac{T_{\mathrm{h,in}} - T_{\mathrm{h,out}}}{\ln\left(\frac{T_{\mathrm{h,in}} - T_s}{T_{\mathrm{h,out}} - T_s}\right)}, \qquad \Delta T_{\mathrm{LM},c} = \frac{T_{c,\mathrm{out}} - T_{c,\mathrm{in}}}{\ln\left(\frac{T_s - T_{c,\mathrm{in}}}{T_s - T_{c,\mathrm{out}}}\right)} \tag{3.30}$$

where $T_{\mathrm{h,in}}$ and $T_{\mathrm{h,out}}$ are the bulk temperatures of the hot fluid at inlet and outlet (K), $T_{c,\mathrm{in}}$ and $T_{c,\mathrm{out}}$ those of the cold fluid (K), and T_s is the (assumed nearly uniform) surface temperature of the separating wall (K). When the wall conductivity is large in directions that distribute heat rapidly, T_s may be treated as spatially uniform and the LMTD above is well defined (Shah & London, 1978). The use of bulk mean temperatures rather than porous-volume averages facilitates direct comparison of the convective coefficient h for TPMS cores with values published for conventional internal geometry for this reason the bulk-temperature definition is adopted in the present study.

Because the LMTD formulation produces a flux-averaged driving temperature in system-level evaluation, overall heat transfer rate $\dot{Q}$ and the overall heat-transfer coefficient U are relevant:

$$\dot{Q} = U A \, \Delta T_{\mathrm{LMTD}} \quad [\mathrm{W}] \tag{3.31}$$

$$\Delta T_{\mathrm{LMTD,tot}} = \frac{(T_{\mathrm{h,in}} - T_{c,\mathrm{out}}) - (T_{\mathrm{h,out}} - T_{c,\mathrm{in}})}{\ln\left(\frac{T_{\mathrm{h,in}} - T_{c,\mathrm{out}}}{T_{\mathrm{h,out}} - T_{c,\mathrm{in}}}\right)} \tag{3.32}$$

Where;

A= the external exchange area [m ^{2}] and;

ΔT_{LMTD} = Log-mean temperature difference for the heat-exchanger configuration.

The overall thermal resistance R_t, is useful for determining the overall heat transfer coefficient V. The relationship is;

$$R_t = \frac{1}{UA} = R_{\{h,conv\}} + R_{\{cond\}} + R_{\{c,conv\}} \tag{3.33}$$

Or equivalently;

$$UA = \frac{1}{\left[\left(\frac{1}{h_h A_h}\right) + \left(\frac{\lambda}{k\ A_s}\right) + \left(\frac{1}{h_c A_c}\right)\right]} \tag{3.34}$$

Where;

$R_{\{h,conv\}} = \frac{1}{h_h A_h}$ = thermal resistance due to convection from the hot fluid,

$R_{\{cond\}} = \frac{\lambda}{k\ A_s}$ = thermal resistance due to conduction through the solid wall and;

$R_{\{c,conv\}} = \frac{1}{h_c A_c}$ = thermal resistance due to convection from the cold fluid.

The NTU (number of transfer units) method is used when embedding TPMS cores into larger systems. The effectiveness ε is defined as the ratio of the actual heat transfer rate to the maximum possible heat transfer rate if the fluid with the minimum heat capacity were to undergo the maximum possible temperature change, where:

$$\varepsilon = \frac{\dot{Q}}{\dot{Q}_{\max}} \tag{3.35}$$

$$\dot{Q}_{\max} = \dot{m}_{\min} c_{p,\min}\left(T_{h,\text{in}} - T_{c,\text{in}}\right) \tag{3.36}$$

$$\text{NTU} = \frac{UA}{\dot{m}\ c_p} \tag{3.37}$$

$$\varepsilon=\frac{1-e^{-\mathrm{NTU}(1-C_r)}}{1-C_r e^{-\mathrm{NTU}(1-C_r)}} \tag{3.38}$$

Where;

$\dot{m}$ = mass flow rate and;

$C_r=C_{\min}/C_{\max}$ = capacity ratio.

These system metrics translate pore-scale improvements in h to device-level thermal performance and allow TPMS designs to be compared in the context of broader thermal systems (Incropera & DeWitt, 2011).

The complex flow path within TPMS geometries is best approximated as a counter-cross flow. In actual evaluation a correction factor is applied, which quantifies the deviation from an ideal counter-flow. A more direct method for representing thermal performance is by using the Temperature Effectiveness, given by

$$\varepsilon = \frac{T_{c,out} - T_{c,in}}{T_{h,in} - T_{c,in}} \tag{3.39}$$

3.6. EXERGY DESTRUCTION

First-law metrics such as Nu and PEC are essential but do not measure irreversibility directly. Second-law analysis, exergy destruction provides insight into whether losses arise more from thermal gradients or from viscous dissipation. The streamwise exergy balance may be written as the difference between inlet and outlet exergy fluxes and the exergy destruction inside the control volume:

$$\dot{E}_d=\sum_{\text{inlets}} \dot{m}_i\,(\mathrm{h}_i-T_0 s_i)-\sum_{\text{outlets}} \dot{m}_o\,(\mathrm{h}_o-T_0 s_o) \tag{3.40}$$

Where;

h = specific enthalpy [J kg $^{-1}$]

s = specific entropy [J kg $^{-1}$ K $^{-1}$]

T_0 = reference temperature [K].

CHAPTER 4

RESULTS AND DISCUSSIONS

This chapter presents the results obtained from the simulations based on the methodology described in the preceding chapter. The accuracy and reliability of the procedures. Thereafter, analytical performance metrics are derived from the simulated data to evaluate the thermal and hydraulic characteristics of the system. The TPMS heat exchanger is then compared with a conventional plate-type heat exchanger, focusing primarily on pressure drop performance. Finally, a comprehensive discussion of the results is provided, highlighting key performance trends, trade-offs, and design implications for potential engineering applications.

4.1. VALIDATION OF SIMULATED HEAT EXCHANGER MODELS

The accuracy of the numerical model developed in ANSYS Fluent for the gyroid-type heat exchanger was established through two complementary approaches; Grid Independence Testing using Richardson extrapolation, and literature-based validation against established graphs of the Nusselt number and pressure drop

4.1.1. GRID INDEPENDENCE TEST RESULTS

A grid independence study was carried out to ensure that the numerical results were not significantly influenced by the mesh resolution. The study was performed on the Gyroid Heat Exchanger using three different mesh densities generated in ANSYS Fluent meshing parameters. All three mesh cases were simulated using identical boundary conditions, fluid properties, and solver settings until a fully converged solution was achieved.

The results of the grid independence study are summarized in the table below;

Table 4.1: *Grid independence test results*

Mesh	Size (mm)	Pressure Drops (Pa)
Fine	5	507.7
Medium	7.07	517.7
Coarse	10	537.7

The Medium mesh was determined to have achieved grid independence at 4.83%, indicating that further mesh refinement no longer produced significant changes in the results. Consequently, the Medium mesh was adopted for all subsequent simulations, as it offers an effective compromise between numerical accuracy and computational efficiency, avoiding the substantial increase in time and resources required for the Fine mesh.

4.1.2. LITERATURE VALIDATION

The computational framework was validated against established literature to ensure physical accuracy

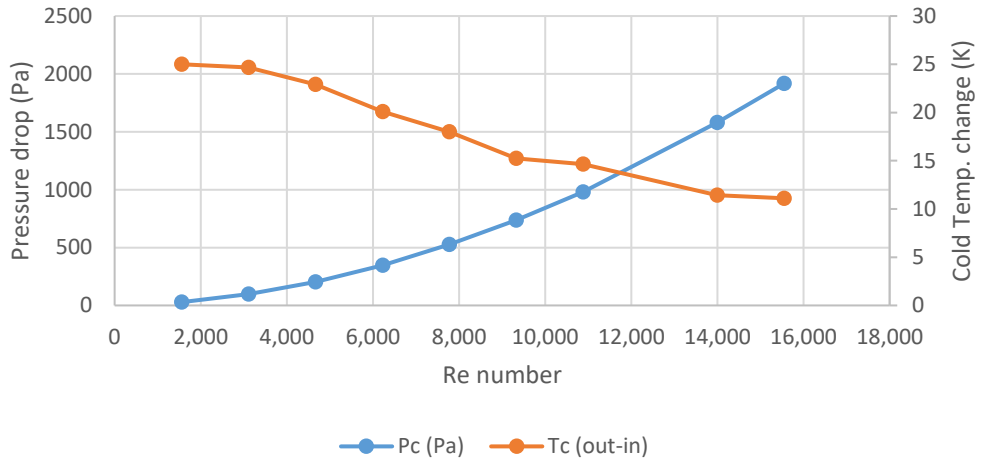

Figure 4.1: *Graph of Pressure drop and cold temperature change against Reynolds*

The results from the simulation show agreement with the trends shown in the paper by Kus et al. (2024).

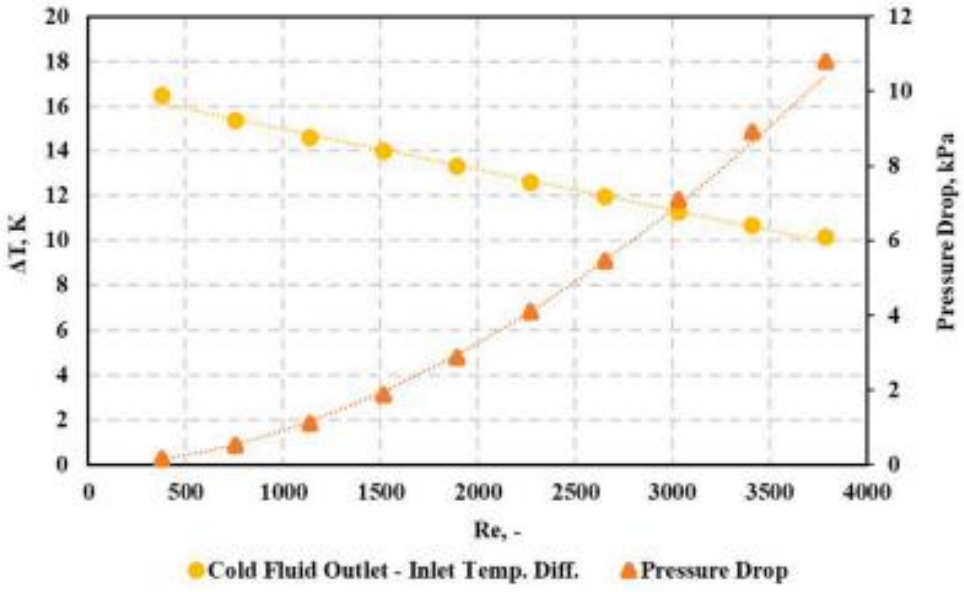

Figure 4.2: *Graph of Pressure drop and cold temperature change against Reynolds from Kus et al. (2024)*

Therefore, the model is deemed sufficiently accurate for conducting an analysis of the Gyroid TPMS heat exchanger's performance.

4.2. ANALYTICAL HEAT EXCHANGER PERFORMANCE EVALUATION RESULTS

Analytical performance evaluation was conducted to quantify the thermal and hydraulic metrics of the gyroid heat exchanger and to interpret the simulated field results in terms of design-level parameters.

Table 4.2: *Simulation results based on varying Mass flow rates*

m (kg/s)	T_{hout} (k)	T_{cout} (k)	S_{hout} (j/kg.k)	S_{cout} (j/kg.k)	h_{hout} (j/kg)	h_{cout} (j/kg)	P_h (pa)	P_c (pa)
0.016667	324.9768	324.9996	502.8089	503.1396	112189.6	112285	29.1716	28.3399
0.0333	325.1231	324.6804	505.2929	498.1258	112801.6	110950.2	93.4461	97.7023

0.05	326.4435	322.9264	524.0458	472.9304	118171.6	103577.1	196.0582	203.656
0.0667	329.0937	320.0912	560.1911	434.7763	129045.5	91757.99	336.0472	346.5596
0.0833	331.2956	317.9821	588.7699	402.2343	138615	82937.73	521.6948	525.6701
0.1	334.3093	315.2354	625.249	372.5503	151218.2	71450.94	712.907	737.822
0.11667	335.5024	314.6625	629.4225	3762.647	152025.7	69055.12	967.3926	980.574
0.15	338.5922	311.4258	674.7585	324.4092	169129.3	55519.32	1509.161	1580.533
0.1667	338.9136	311.1093	679.5088	319.7503	170473.6	54195.61	1845.702	1917.064

4.2.1. THERMAL PERFORMANCE METRICS

The thermal performance of the gyroid TPMS heat exchanger was evaluated using three key parameters: Thermal Effectiveness, Number of Transfer Units, Overall Heat Transfer Coefficient, and the Colburn *j*-factor. These metrics were obtained from post-processed simulation data in ANSYS Fluent.

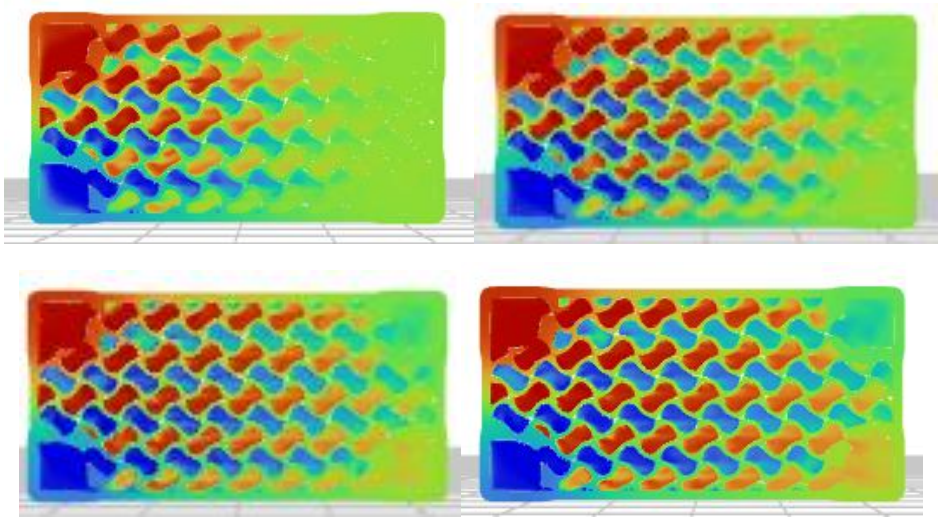

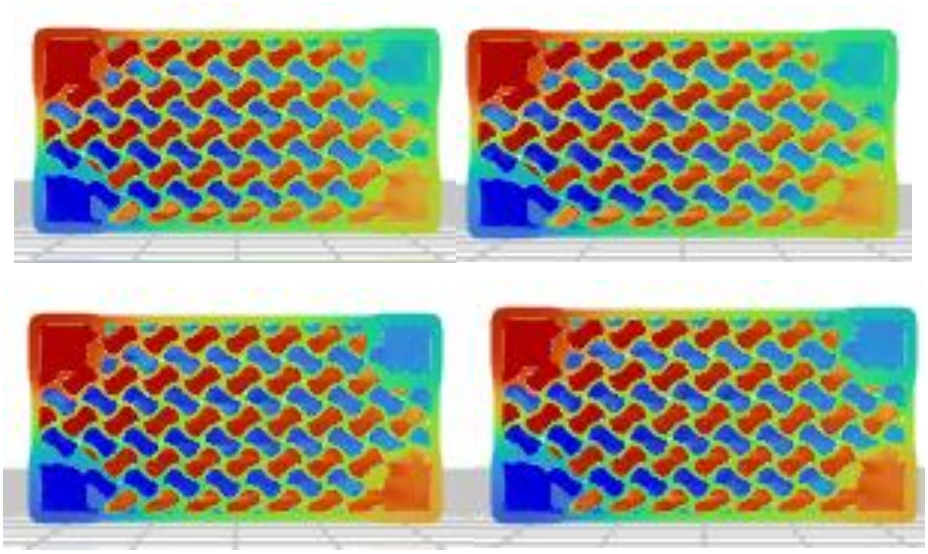

Figure 4.3 *Temperature contours of mass flow rate xx through the cross-section in the XY symmetry plane*

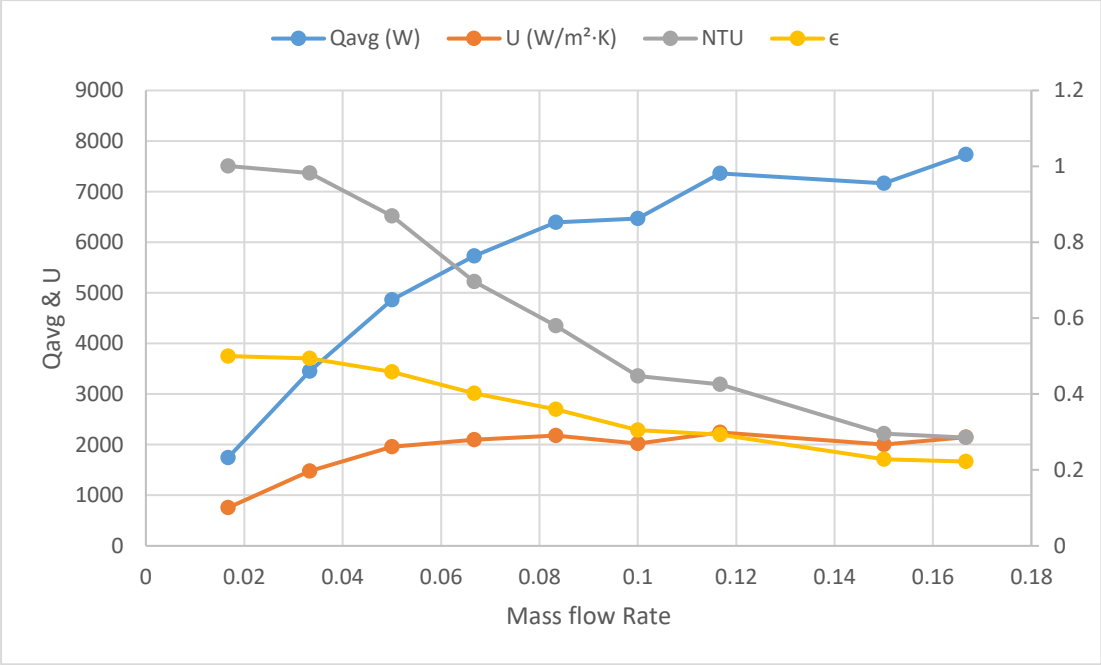

Figure 4.4: *Graph of Q, U, NTU and Effectiveness against Mass flow Rate*

The thermal performance of the gyroid TPMS heat exchanger shows a clear trade-off as mass flow rate increases. The average heat transfer rate (Qavg) and the overall heat transfer coefficient (U) both increase. This is because higher flow rates transport more energy and the increased turbulence enhances the convective heat transfer.

Conversely, the heat exchanger effectiveness (ε) and the Number of Transfer Units (NTU) both decrease. This is caused by the reduced fluid residence time, which lowers the thermal efficiency (ε), and the fact that the heat capacity rate increases faster than the U-value, thus lowering the NTU. The relationship is also validated by Kus et al., where an increase in NTU resulted in an increase in effectiveness.

This behaviour underscores a necessary compromise: increasing the flow rate amplifies the total heat transfer power but does so at the cost of thermal effectiveness.

4.2.2. HYDRAULIC AND COMBINED PERFORMANCE METRICS

The hydraulic characteristics of the gyroid heat exchanger were also evaluated, focusing on pressure drop, friction factor, and pumping power, which together determine the flow resistance and energy required to drive the fluids through the exchanger.

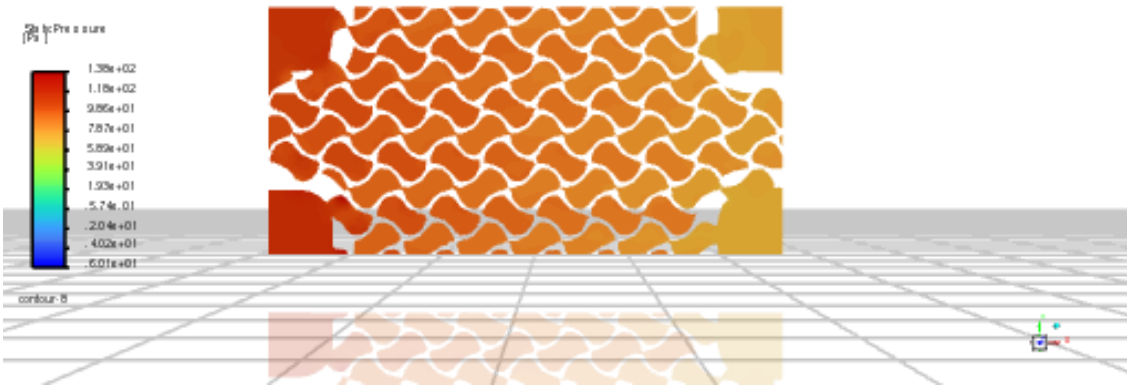

Figure 4.5: *Pressure contour of through the cross-section in the XY symmetry plane*

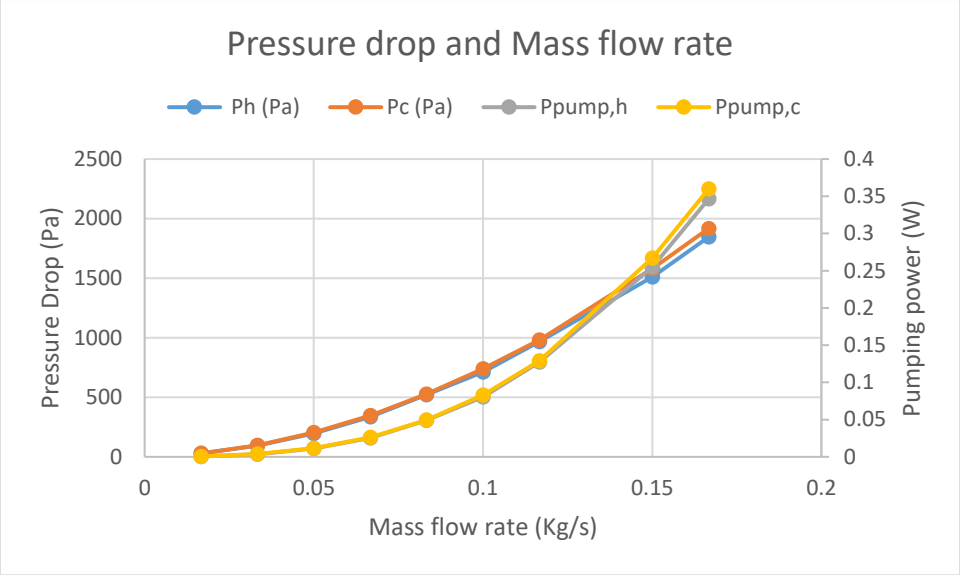

Figure 4.6: *Graph of Pressure Drop vs Mass flow Rate*

This chart plots the simulated pressure drop (in Pa) and Pumping power (W) against the mass flow rate (in Kg/s) for both the hot and cold fluid channels of the heat exchanger.

The data confirms the fundamental relationship between these variables. Both the hot and cold sides exhibit a non-linear, quadratic (parabolic) trend. The pressure drop does not increase linearly; it increases exponentially as the mass flow rate rises. For example, there is an 380% increase in pressure drop at 0.1 Kg/s compared to the drop at 0.05 Kg/s. The Pressure drop scales with Re as expected in laminar and turbulent regions which agres with the Darcy-Weisbach relation in equation 3.22. Since mass flow rate is directly proportional to velocity in a channel of fixed area, it follows that the pressure drop is proportional to the square of the mass flow rate.

A notable observation is that the Ph and Pc curves are nearly identical, lying almost perfectly on top of each other. This suggests a well-balanced heat exchanger design, where the hydraulic characteristics and geometric flow paths for both the hot and cold fluids are equivalent, resulting in the same hydraulic resistance.

The chart also illustrates the pumping power penalty. While the previous thermal analysis showed that a higher mass flow rate increases the total heat transfer (Qavg), it does not come without the significant cost. To achieve a small increase in flow rate at the high end (e.g., from 0.15 to 0.17 Kg/s), a disproportionately large increase in pressure is required, which in turn demands a significant increase in pumping power.

4.2.3. PERFORMANCE EVALUATION CRITERION

To evaluate the overall performance balance between thermal enhancement and hydraulic penalty, the Performance Evaluation Criterion (PEC) was used.

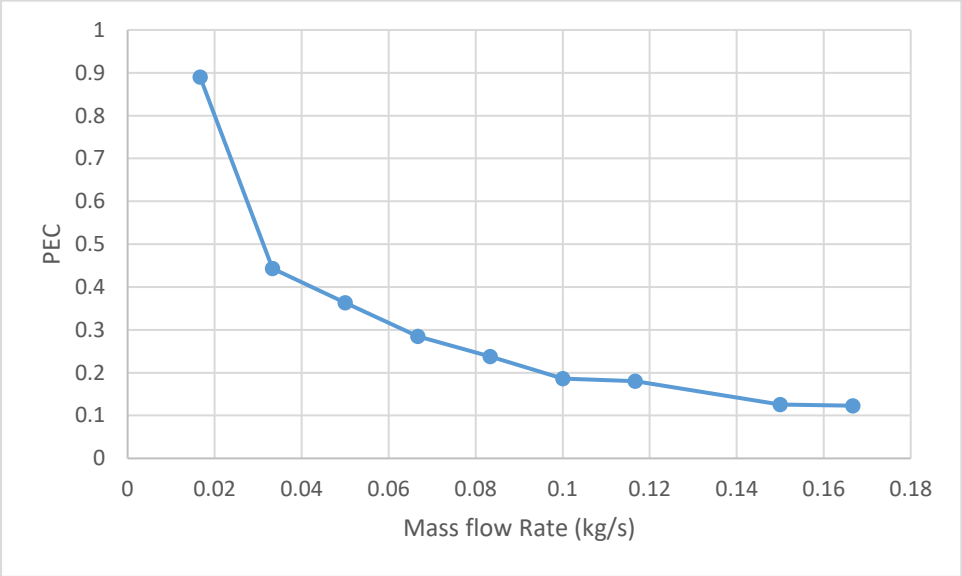

Figure 4.7: *Graph of PEC against Mass flow Rate*

The chart describes a strong, inverse relationship between the PEC and the mass flow rate. The PEC achieves its maximum value at the lowest tested mass flow rate Kg/s. As the mass flow rate increases, the PEC drops sharply, eventually levelling off at a low value of approximately 0.12 at the highest flow rates.

This trend is a direct consequence of the competing physics. The cost which is the pressure drop, increases quadratically with the mass flow rate. In contrast, the benefit, convective heat transfer, related to Nu increases at a much slower, sub-quadratic rate. Because the denominator (cost) in the PEC calculation grows much faster than the numerator (benefit), the overall ratio continuously decreases.

The primary implication is that the gyroid TPMS heat exchanger is most worth it at low flow rates, where the frictional penalty is small. As the flow rate increases to achieve higher total heat transfer (Qavg), the system becomes progressively less efficient from a thermo-hydraulic standpoint.

Furthermore, it is critical to note that the PEC value never exceeds 1.0 across the entire tested range. This suggests that for this specific design and set of operating

conditions, the massive increase in friction caused by the complex gyroid structure is always more significant than the thermal enhancement it provides, when compared to the baseline. Therefore, while effective at transferring heat, it does so at a high and inefficient pumping power cost.

4.3. EXERGY DESTRUCTION

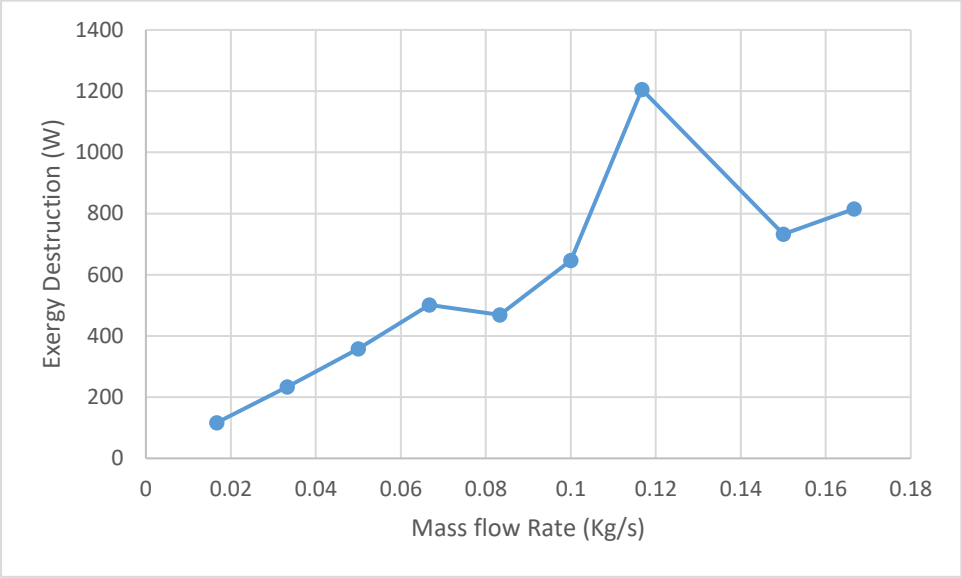

Figure 4.8: *Graph of Exergy Destruction against Mass flow rate*

The chart describes the real-world thermodynamic inefficiency of the gyroid TPMS heat exchanger. As the mass flow rate increases, the exergy destruction rises steeply from a low point,110 W at 0.02 Kg/s to a distinct peak of approximately 1200 W at a mass flow rate of 0.12 Kg/s. Beyond this peak, the total exergy destruction begins to decline, falling to around 810 W at 0.17 Kg/s.

This peak does not represent an optimal condition; rather, it signifies the point of maximum thermodynamic inefficiency, which is the worst operating point for the system.

This behaviour is understood as the sum of the competing thermal and hydraulic (frictional) irreversibilities. At low mass flow rates, the minimal pressure drop results in small frictional irreversibility. However, as the flow rate increases, the pressure drop increases quadratically, causing the frictional exergy destruction to rise

exponentially. Concurrently, thermal irreversibility also changes with the flow rate due to varying residence times and temperature profiles. The peak at 0.12 Kg/s represents the flow rate where the combined effect of these two loss mechanisms is at its maximum.

The subsequent decline suggests that changes in the thermal profile can be related to the sharp decrease in thermal effectiveness at high flow rates which begin to reduce the thermal irreversibility at a rate that is more significant than the continued rise in frictional irreversibility.

From a real-world design perspective, this analysis is crucial as it demonstrates the operating points that maximize heat transfer (high flow rates) and minimize pressure drop (low flow rates) do not necessarily align with the point of maximum thermodynamic efficiency. The exergy analysis identifies a specific operating region, centred around 0.12 Kg/s, that should be actively avoided due to its excessive destruction of useful energy. The true optimal design point is therefore a compromise, balancing the objective of high heat transfer (Qavg) against the costs of pumping power and thermodynamic losses (exergy destruction).

4.4. COMPARISON WITH PLATE TYPE HEAT EXCHANGER

To contextualize the performance of the simulated TPMS gyroid, its results at a mass flow rate of 0.1kg/s were compared against data for a conventional plate-type heat exchanger BT3x8-20 operating at a similar inlet and outlet conditions sourced from literature. This comparison highlights the fundamental design trade-offs between the two technologies. The key parameters are summarized in the table below:

Table 4.3: *Performance Comparison*

Parameter	TPMS Gyroid Hx (Simulated)	Plate-Type HX (BT3x Data)
Heat Transfer Area (A)	0.221 m²	0.235 m²
Total Heat Transfer (Q_{avg})	6,467 W	15,500 W
Overall Coefficient (U)	848 W/m²·K	2,583 W/m²·K

Cold-Side Pressure Drop (Pc)	738 Pa	10,103 Pa
LMTD	34.54 K	25.99 K

This comparison provides a clearer insight into the design trade-offs:

1. Heat Transfer Performance: The plate heat exchanger outperforms the TPMS heat exchanger in terms of raw thermal performance.
   i. It transfers 2.4 times more heat, 15,500 W vs. 6,467 W.
   ii. Since the areas are nearly identical, its performance per area (heat flux) is also 2.25 times higher.
   iii. This is driven by a superior Overall Heat Transfer Coefficient (U), which is 3 times higher than the TPMS's

This aligns perfectly with the calculated PEC value of 0.186. A PEC this low indicates that the TPMS, for its given size, is not an effective design for maximizing total heat transfer.

2. Hydrodynamic (Pumping) Performance:

The TPMS gyroid is the clear winner in terms of efficiency as Its pressure drop is 1370% lower than the plate heat exchanger's; 738 Pa vs 10,103Pa.

To quantify this, comparison of their Pumping Efficiency (heat transferred per unit of pressure drop) shows that;

TPMS Gyroid Hx:

$$\frac{Q}{P_c} = \frac{6{,}467\ W}{738\ pa} = 8.76\ W/Pa$$

Plate HX:

$$\frac{Q}{P_c} = \frac{15{,}500W}{10{,}103\ pa} = 1.53\ W/Pa$$

Therefore, the TPMS gyroid is 5.7 times more efficient in its use of pumping power. With similar areas, the comparison is a direct trade-off between power and efficiency.

The Plate HX is a brute force design where it achieves high heat transfer by forcing fluid through a high-resistance path, resulting in excellent thermal performance at the cost of massive pumping power.

The TPMS Gyroid HX is a high efficiency design offering a low-drag, low-resistance path that, while less effective at transferring total heat, does so with a fraction of the required pumping power.

This makes the TPMS design suitable for applications where minimizing pump size and energy consumption is more important than achieving the maximum possible heat transfer in a given volume.

CHAPTER 5

CONCLUSION

The research attempted to design and analyse the thermal-hydraulic performance of a Gyroid core TPMS heat exchanger for commercial applications. CFD analysis using the k-ω Shear Stress Transport (SST) turbulent model and conjugate heat transfer (CHT) were used to investigate the characteristics of flow and the properties of heat transfer in the TPMS based heat exchangers.

The workflow starts by generating the heat exchanger geometry in nTop, which incorporates mathematically defined core structures, namely, TPMS structures, as the heat transfer medium. The heat exchanger geometry is then export to Ansys Fluent for CFD analysis with the aid of Fault Tolerance Meshing (FTM), suitable for complex geometries such as TPMS cores.

A significant hurdle in this analysis was the computationally demanding task of meshing the gyroid's complex geometry. To ensure the findings were reliable, a rigorous grid independence test was performed. This essential procedure validated the final CFD model by confirming that the results were not sensitive to the mesh density, thereby establishing a balance between computational effort and solution accuracy.

Analysis of the CFD results showed that the heat transfer performance of TPMS structures is directly related to their geometric properties such as porosity, hydraulic diameter, and solid to fluid interaction area. Although determining the solid to fluid interaction area of complex shapes like TPMS structures can be challenging, with the use of meshing tools, approximate values can be calculated. Pressure drop estimations can be performed using analytical friction factor formulas (Equation 3.22) together with friction factor correlations for TPMS structures in the literature.

Comparison between simulated Gyroid-based design and conventional Plate type design showed a distinct trade-off. The plate-type Hx demonstrated significantly higher thermal performance, transferring 2.4 times more heat and possessing an overall heat transfer coefficient three times greater. However, this superior heat transfer was achieved at the cost of a substantial pressure drop. In contrast, the TPMS gyroid proved to be the more efficient design hydrodynamically, exhibiting a pressure drop 13.7 times lower. This efficiency translates to the TPMS gyroid using 5.7 times less pumping

power for the heat it transfers, making it an ideal choice for applications where operational energy cost and pump size are more critical design constraints than raw thermal output.

5.1. RECOMMENDATIONS

Based on the concept and results of the project, the following recommendations are proposed to enhance future research in TPMS Heat Exchanger design and analysis

1. To reduce reliance on computationally expensive CFD simulations future studies should focus on the development on empirical and semi-empirical correlations from validated CFD or experimental datasets which would serve as reduced-order models enabling rapid assessment of thermo hydraulic parameters This approach would greatly enhance design efficiency and make TPMS core analysis more accessible for practical engineering applications.
2. Collaborations among academia, industry, and CFD software developers such be formally established. Academic partnerships provide theoretical and experimental depth and access to relevant journals, industrial collaborations bring real-world performance insights and scalability perspectives, while engagement with CFD software developers can foster custom tool development for TPMS generation and analysis. Such interdisciplinary synergy is essential for transitioning research into viable engineering solutions.
3. TPMS Heat Exchangers should be evaluated across diverse working fluids, as thermal and hydraulic characteristics are strongly dependent on fluid properties such as viscosity and density. Testing with water-glycol mixtures, refrigerants, oils, and other relevant fluids will establish a broader performance range and enhance the applicability of TPMS designs in automotive, aerospace, and energy systems.
4. Mainstream deployment of TPMS cores in commercial heat exchanger systems. This requires progression from laboratory-scale experiments to pilot-scale demonstrations within operational environments such as waste heat recovery. Long-duration reliability tests and accelerated life-cycle assessments should be performed to validate durability and establish confidence among potential industrial adopters.
5. Computational models must evolve to account for real-world physical effects that influence TPMS performance. This includes the impact of surface roughness resulting from additive manufacturing, fouling or scaling during extended operation, and structural anisotropy inherent in printed materials. Integrating these

phenomena into simulations will narrow the gap between predicted and experimental results, improving the accuracy and reliability of performance forecasts.

6. Design exploration should be guided by the field synergy principle, which emphasizes maximizing the alignment between velocity and temperature gradients to enhance convective heat transfer. Achieving this requires a deeper understanding of how the local flow topology within TPMS structures governs energy transport. By integrating flow visualization, entropy generation analysis, and field synergy evaluation, valuable insights can be gained into how geometric parameters such as cell size, wall thickness, porosity through cell stretching, and local scaling within TPMS generation algorithms, as well as using affect both local heat transfer enhancement and overall thermal effectiveness. Such an approach enables spatial tailoring of flow resistance and heat transfer characteristics for optimized thermal performance.

REFERENCES

Al-Ketan, O., & Abu Al-Rub, R. K. (2019). Multifunctional Mechanical Metamaterials Based on Triply Periodic Minimal Surface Lattices. In *Advanced Engineering Materials* (Vol. 21, Issue 10). Wiley-VCH Verlag. https://doi.org/10.1002/adem.201900524

Al-Ketan, O., Ali, M., Khalil, M., Rowshan, R., Khan, K. A., & Abu Al-Rub, R. K. (2021). Forced Convection Computational Fluid Dynamics Analysis of Architected and Three-Dimensional Printable Heat Sinks Based on Triply Periodic Minimal Surfaces. *Journal of Thermal Science and Engineering Applications*, *13*(2). https://doi.org/10.1115/1.4047385/1084162

Asif, M., & Grande, C. A. (2022). TPMS Contactors Designed with Imprinted Porosity: Numerical Evaluation of Momentum and Energy Transport. *Industrial & Engineering Chemistry Research, 61*(50), 18556–18566. https://doi.org/10.1021/ACS.IECR.2C03384

Attarzadeh, R., Attarzadeh-Niaki, S. H., & Duwig, C. (2022). Multi-objective optimization of TPMS-based heat exchangers for low-temperature waste heat recovery. *Applied Thermal Engineering, 212*. https://doi.org/10.1016/j.applthermaleng.2022.118448

Attarzadeh, R., Rovira, M., & Duwig, C. (2021). Design analysis of the “Schwartz D” based heat exchanger: A numerical study. *International Journal of Heat and Mass Transfer, 177*, 121415. https://doi.org/10.1016/J.IJHEATMASSTRANSFER.2021.121415

Baena-Moreno, F. M., González-Castaño, M., Navarro De Miguel, J. C., Miah, K. U. M., Ossenbrink, R., Odriozola, J. A., & Arellano-García, H. (2021). Stepping toward Efficient Microreactors for CO2 Methanation: 3D-Printed Gyroid Geometry. *ACS Sustainable Chemistry and Engineering, 9*(24), 8198–8206. https://doi.org/10.1021/ACSSUSCHEMENG.1C01980

Baobaid, N., Ali, M. I., Khan, K. A., & Abu Al-Rub, R. K. (2022). Fluid flow and heat transfer of porous TPMS architected heat sinks in free convection environment. *Case*

Studies in Thermal Engineering, *33*, 101944. https://doi.org/10.1016/J.CSITE.2022.101944

Barakat, A., & Sun, B. B. (2024). Enhanced convective heat transfer in new triply periodic minimal surface structures: Numerical and experimental investigation. *International Journal of Heat and Mass Transfer*, *227*, 125538. https://doi.org/10.1016/J.IJHEATMASSTRANSFER.2024.125538

Bayomy, A. M. (2017). Electronic Cooling Using ERG Aluminium Foam Subjected to Steady/ Pulsating Water and γ-Al2O3–Water Nanofluid Flows: Experimental and Numerical Approach [Ph.D. Thesis, Ryerson University].

Beer, M., & Rybár, R. (2024). Optimisation of Heat Exchanger Performance Using Modified Gyroid-Based TPMS Structures. *Processes,* *12*(12). https://doi.org/10.3390/pr12122943

Bhattacharya, A., Calmidi, V. v, & Mahajan, R. L. (2021). Thermophysical properties of high porosity metal foams. www.elsevier.com/locate/ijhmt

Brambati, G., Guilizzoni, M., & Foletti, S. (2024). Convective heat transfer correlations for Triply Periodic Minimal Surfaces based heat exchangers. *Applied Thermal Engineering, 242*. https://doi.org/10.1016/j.applthermaleng.2024.122492

Careri, F., Khan, R. H. U., Todd, C., & Attallah, M. M. (2023). Additive manufacturing of heat exchangers in aerospace applications: a review. *Applied Thermal Engineering*, *235*, 121387. https://doi.org/10.1016/j.applthermaleng.2023.121387

Delalic, N., Mulahasanovic, D., & Ganic, E. N. (2004). Porous media compact heat exchanger unit—experiment and analysis. *Experimental Thermal and Fluid Science*, *28*(2–3), 185–192. https://doi.org/10.1016/S0894-1777(03)00038-4

Deshmukh, S., Ronge, H., & Ramamoorthy, S. (2019). Design of periodic foam structures for acoustic applications: Concept, parametric study and experimental validation. *Materials and Design,* *175*. https://doi.org/10.1016/J.MATDES.2019.107830

Ding, J., Zou, Q., Qu, S., Bartolo, P., Song, X., & Wang, C. C. L. (2021). STL-free design and manufacturing paradigm for high-precision powder bed fusion. *CIRP Annals*, *70*(1), 167–170. https://doi.org/10.1016/J.CIRP.2021.03.012

Feng, J., Fu, J., Yao, X., & He, Y. (2022). Triply periodic minimal surface (TPMS) porous structures: From multi-scale design, precise additive manufacturing to multidisciplinary applications. In *International Journal of Extreme Manufacturing* (Vol. 4, Issue 2). IOP Publishing Ltd. https://doi.org/10.1088/2631-7990/ac5be6

Fu, Z. Xu, G. Panagakos, CFD study of countercurrent flow in triply periodic minimal surfaces with CO2BOL solvent, Pacific Northwest National Laboratory, Richland, USA, 2019 https://www.osti.gov/biblio/1691506-cfd-studycountercurrent-flow-triply-periodic-minimal-surfaces-co2bol-solvent.

Gao, F., Peng, H., & Hu, W. (n.d.). *DESIGN, MODELING AND CHARACTERIZATION OF TRIPLY PERIODIC MINIMAL SURFACE HEAT EXCHANGERS WITH ADDITIVE MANUFACTURING*. https://www.researchgate.net/publication/340077269

Giannitelli, S. M., Accoto, D., Trombetta, M., & Rainer, A. (2014). Current trends in the design of scaffolds for computer-aided tissue engineering. *Acta Biomaterialia, 10*(2), 580–594. https://doi.org/10.1016/J.ACTBIO.2013.10.024

Guo, Z. Y., Li, D. Y., & Wang, B. X. (1998). A novel concept for convective heat transfer enhancement. *Int. J. Heat Mass Transf., 41*(14), 2221–2225.

Hawken, M. B., Reid, S., Clarke, D. A., Watson, M., Fee, C. J., & Holland, D. J. (2023). Characterization of pressure drop through Schwarz-Diamond triply periodic minimal surface porous media. *Chemical Engineering Science, 280*. https://doi.org/10.1016/j.ces.2023.119039

Herz, A., Malayeri, M. R., & Müller-Steinhagen, H. (2008). Fouling of roughened stainless steel surfaces during convective heat transfer to aqueous solutions. *Energy Conversion and Management*, *49*(11), 3381–3386. https://doi.org/10.1016/J.ENCONMAN.2007.09.034

Ibhadode, O. (2024). The effects of cell stretching on the thermal and flow characteristics of triply periodic minimal surfaces. *International Communications in Heat and Mass Transfer, 153*. https://doi.org/10.1016/j.icheatmasstransfer.2024.107364

Incropera, F. P., & DeWitt, D. P. (2007). *Fundamentals of Heat and Mass Transfer* (6th ed.). Wiley.

Incropera, F.P. and Dewitt, D.P. (2011) Fundamentals of Heat and Mass Transfer. 7th Edition, John Wiley & Sons, Inc.

Iyer, J., Moore, T., Nguyen, D., Roy, P., & Stolaroff, J. (2022). Heat transfer and pressure drop characteristics of heat exchangers based on triply periodic minimal and periodic nodal surfaces. *Applied Thermal Engineering, 209*, 118192. https://doi.org/10.1016/J.APPLTHERMALENG.2022.118192

Jiang, W., Liao, W., Liu, T., Shi, X., Wang, C., Qi, J., Chen, Y., Wang, Z., & Zhang, C. (2021). A voxel-based method of multiscale mechanical property optimization for the design of graded TPMS structures. *Materials and Design, 204*. https://doi.org/10.1016/j.matdes.2021.109655

Jung, Y., & Torquato, S. (2005). Fluid permeabilities of triply periodic minimal surfaces. *Physical Review. E, Statistical, Nonlinear, and Soft Matter Physics*, *72*(5 Pt 2). https://doi.org/10.1103/PHYSREVE.72.056319

Kaviany, M. (1995). Convection Heat Transfer. In: *Principles of Heat Transfer in Porous Media*. Mechanical Engineering Series. Springer, New York, NY. https://doi.org/10.1007/978-1-4612-4254-3_4

Kays, W.M., & London, A.L. (1984). *Compact heat exchangers* (3rd ed.). McGraw Hill.

Khrapov, D., Kozadayeva, M., Manabaev, K., Panin, A., Sjöström, W., Koptyug, A., Mishurova, T., Evsevleev, S., Meinel, D., Bruno, G., Cheneler, D., Surmenev, R., & Surmeneva, M. (2021). Different approaches for manufacturing ti-6al-4v alloy with triply periodic minimal surface sheet-based structures by electron beam melting. *Materials, 14*(17). https://doi.org/10.3390/ma14174912

King, W. E., Anderson, A. T., Ferencz, R. M., Hodge, N. E., Kamath, C., Khairallah, S. A., & Rubenchik, A. M. (2015). Laser powder bed fusion additive manufacturing of metals; physics, computational, and materials challenges. *Applied Physics Reviews, 2*(4), 041304. https://doi.org/10.1063/1.4937809

Kumar, P., & Fernández, E. (2022). *Topology optimization for additive manufacturing with length scale, overhang, and building orientation constraints*. http://arxiv.org/abs/2204.07333

Kus, K., Wójcik, M., Malecha, Z., & Rogala, Z. (2024). Numerical and experimental investigation of the gyroid heat exchanger. *International Journal of Heat and Mass Transfer, 231*. https://doi.org/10.1016/j.ijheatmasstransfer.2024.125882

Kwasi-Effah, C. C., Ibhadode, O., & Qureshi, A. (2024). Thermo-hydraulic performance characteristics of novel G-Prime and FRD Triply Periodic Minimal Surface (TPMS) geometries. *International Communications in Heat and Mass Transfer, 159*. https://doi.org/10.1016/j.icheatmasstransfer.2024.108226

Li, W., Li, W., & Yu, Z. (2022). Heat transfer enhancement of water-cooled triply periodic minimal surface heat exchangers. *Applied Thermal Engineering, 217*. https://doi.org/10.1016/j.applthermaleng.2022.119198

Li, W., Yu, G., & Yu, Z. (2020). Bioinspired heat exchangers based on triply periodic minimal surfaces for supercritical CO2 cycles. *Applied Thermal Engineering, 179*. https://doi.org/10.1016/j.applthermaleng.2020.115686

Lu, T. J., Stone, H. A., & Ashby, M. F. (1998). Heat transfer in open-cell metal foams. *Acta Materialia, 46*(10), 3619–3635. https://doi.org/10.1016/S1359-6454(98)00031-7

Lyu, Y., Gong, T., He, T., Wang, H., Zhuravkov, M., & Xia, Y. (2024). Study on the Energy Absorption Performance of Triply Periodic Minimal Surface (TPMS) Structures at Different Load-Bearing Angles. *Biomimetics*, *9*(7), 392. https://doi.org/10.3390/biomimetics9070392

Maconachie, T., Leary, M., Lozanovski, B., Zhang, X., Qian, M., Faruque, O., & Brandt, M. (2019). SLM lattice structures: Properties, performance, applications and

challenges. *Materials & Design, 183*, 108137. https://doi.org/10.1016/J.MATDES.2019.108137

Novak, N., Borovinšek, M., Al-Ketan, O., Ren, Z., & Vesenjak, M. (2022). Impact and blast resistance of uniform and graded sandwich panels with TPMS cellular structures. *Composite Structures*, *300*, 116174. https://doi.org/10.1016/j.compstruct.2022.116174

Piedra, S., Gómez-Ortega, A., & Pérez-Barrera, J. (2023). Prediction of Flow Properties of Porous Triply Periodic Minimal Surface (TPMS) Structures. *Fluids, 8*(12). https://doi.org/10.3390/fluids8120312

Rathore, S. S., Mehta, B., Kumar, P., & Asfer, M. (2022). Flow Characterization in Triply Periodic Minimal Surface (TPMS)-Based Porous Geometries: Part 1—Hydrodynamics. *Transport in Porous Media 2022 146:3, 146*(3), 669–701. https://doi.org/10.1007/S11242-022-01880-7

Reynolds, B. W., Fee, C. J., Morison, K. R., & Holland, D. J. (2023). Characterisation of Heat Transfer within 3D Printed TPMS Heat Exchangers. *International Journal of Heat and Mass Transfer, 212*. https://doi.org/10.1016/j.ijheatmasstransfer.2023.124264

Röver, T., Kuehne, M., Bischop, F., Clague, L., Bossen, B., & Emmelmann, C. (2023). Design and numerical assessment of an additively manufactured Schwarz diamond triply periodic minimal surface fluid-fluid heat exchanger. *Journal of Laser Applications, 35*(4). https://doi.org/10.2351/7.0001184

Saghir, M. Z., Kerme, E. D., Hajialibabei, M., Rasheed, H., Welsford, C., & Al-Ketan, O. (2024). Study of the Thermal and Hydraulic Performance of Porous Block versus Gyroid Structure: Experimental and Numerical Approaches. *Energies, 17*(4). https://doi.org/10.3390/en17040861

Saghir, M. Z., & Kilic, G. A. (2024). Experimental Forced Convection Study Using a Triply Periodic Minimal Surface Porous Structure with a Nanofluid: Comparison with Numerical Modeling. *Applied Sciences (Switzerland), 14*(17). https://doi.org/10.3390/app14177594

Sharma, D., & Hiremath, S. S. (2022). Bio-inspired repeatable lattice structures for energy absorption: Experimental and finite element study. *Composite Structures, 283*, 115102. https://doi.org/10.1016/J.COMPSTRUCT.2021.115102

Slaughter, V. B. (2006). *Method of using minimal surfaces and minimal skeletons to make heat exchanger components*. https://patents.google.com/patent/US7866377B2

Sun, J., Li, X., Mao, H., Ma, Y., Liu, J., & Chen, X. (2021). ·Numerical analysis of the mechanism of porosity effect on the thermal-hydraulic performance of Gyroid-type TPMS structures in combined aero engines. https://ssrn.com/abstract=4976484

Tang, W., Guo, J., Yang, F., Zeng, L., Wang, X., Liu, W., Zhang, J., Zou, C., Sun, L., Zeng, Y., Zhang, Z., Fu, J., & Zhao, Y. (2024). Performance analysis and optimization of the Gyroid-type triply periodic minimal surface heat sink incorporated with fin structures. *Applied Thermal Engineering, 255*. https://doi.org/10.1016/j.applthermaleng.2024.123950

Tang, W., Zhou, H., Zeng, Y., Yan, M., Jiang, C., Yang, P., Li, Q., Li, Z., Fu, J., Huang, Y., & Zhao, Y. (2023). Analysis on the convective heat transfer process and performance evaluation of Triply Periodic Minimal Surface (TPMS) based on Diamond, Gyroid and Iwp. *International Journal of Heat and Mass Transfer, 201*. https://doi.org/10.1016/j.ijheatmasstransfer.2022.123642

Tang, W., Zou, C., Zhou, H., Zhang, L., Zeng, Y., Sun, L., Zhao, Y., Yan, M., Fu, J., Hu, J., Li, Z., Liu, Z., Wang, T., & Zhang, Z. (2023). A novel convective heat transfer enhancement method based on precise control of Gyroid-type TPMS lattice structure. *Applied Thermal Engineering, 230*. https://doi.org/10.1016/j.applthermaleng.2023.120797

Wang, J., Qian, C., Qiu, X., Yu, B., Yan, L., Shi, J., & Chen, J. (2024). Numerical and experimental investigation of additive manufactured heat exchanger using triply periodic minimal surfaces (TPMS). *Thermal Science and Engineering Progress*, *55*, 103007. https://doi.org/10.1016/J.TSEP.2024.103007

Whitaker, S. (1999a). *The Method of Volume Averaging. 13*. https://doi.org/10.1007/978-94-017-3389-2

Xu, H., Zhang, Y., Mei, Y., Wu, Z., Zhang, Y., Ma, M., & Liu, X. (2025). Hierarchical sheet triply periodic minimal surface lattices: Design, performance and optimization. *Appl. Therm. Eng., 261*, 125187.

Yan, K., Wang, J., Li, L., & Deng, H. (2023). Numerical investigation into thermo-hydraulic characteristics and mixing performance of triply periodic minimal surface-structured heat exchangers. *Applied Thermal Engineering, 230*. https://doi.org/10.1016/j.applthermaleng.2023.120748

Yeranee, K., & Rao, Y. (2022). A Review of Recent Investigations on Flow and Heat Transfer Enhancement in Cooling Channels Embedded with Triply Periodic Minimal Surfaces (TPMS). *Energies, 15*(23), 8994. https://doi.org/10.3390/en15238994

Zhang, F., Wang, J., Qian, C., Shi, J., Yu, B., & Chen, J. (2025). Performance comparison and analysis of gradient-optimized triply periodic minimal surface heat exchangers based on field synergy principle. *Applied Thermal Engineering, 275*. https://doi.org/10.1016/j.applthermaleng.2025.126887